

FACULTY OF PHYSICS "BABEȘ-BOLYAI UNIVERSITY" CLUJ-NAPOCA  
ROMANIA

**STUDY ON THE STRUCTURE, MICROSTRUCTURE AND INTERPHASE  
EXCHANGE COUPLING IN HARD-SOFT MAGNETIC NANOCOMPOSITES**

Răzvan Hirian

Scientific Adviser  
Prof. Dr. Viorel Pop

# Acknowledgments

First of all I would like to extend my sincerest gratitude to Prof. Dr. Viorel Pop, my scientific adviser, for his guidance and his persistent drive to push me to become a better researcher and sometimes a better person.

I would like to also thank the members of the doctoral guidance committee: Prof. Dr. Romulus Tetean, Prof. Dr. Daniel Andreica and Prof. Dr. Iosif Grigore Deac for their support during this time.

Of course, I must thank Prof. Dr. Olivier Isnard from Université Grenoble Alpes and Institut Néel in Grenoble, not only for his willingness to engage in joint projects but also for his guidance along the way, as his words have often driven me to strive to improve. My improved understanding of FORC studies came from Prof. Dr. Alexandru Stancu from Universitatea Alexandru Ioan Cuza in Iași, who was generous enough to have received me in his research group. I thank Prof. Dr. Marin Coldea from Universitatea Babeș-Bolyai, Cluj-Napoca, for the many fruitful discussion on matters of materials science and physics. My gratitude also extends to Prof. Dr. Ionel Chicinaș from Universitatea Tehnică of Cluj-Napoca for his willingness to engage in joint works and for his freely offered advice and knowledge.

This work would not have been possible without the contribution of many other people from our university and other institutions whom I sincerely thank. Bogdan Neamțu, Florin Popa and Cristina Stanciu from Universitatea Tehnică of Cluj-Napoca for their help with sample preparation, structural and microstructural analysis, and often very fruitful discussions. Lucian Barbu-Tudoran from INCDTIM Cluj-Napoca for some of the SEM images contained in this work. From our own institution, Dr. Sever Mican with whom I have worked very closely for many years and whose expertise I have often relied on; Teodor-Lucian Biter and George Crișan for their help in working out the computer simulations contained in this work.

I would like to thank all of my colleagues who helped me out and generally made life bearable. Also, I must include the support staff at Universitatea Babeș-Bolyai Cluj-Napoca and Institut Néel in Grenoble France for all of their help.

Most importantly I must thank my family for their patience and support, which on occasion went above and beyond.

Finally I wish to thank Romanian Ministry of Education and Research for financial support: Grant PN-II-ID-PCE-2012-4-0470, Grant PN-II-RU-TE-2014-4-2360 and Grant PN-II-RU-TE-2014-4-0009.

# Contents

<b>Acknowledgments</b>	<b>ii</b>
<b>1 Introduction</b>	<b>1</b>
1.1 Preamble . . . . .	1
1.2 General Context . . . . .	1
1.2.1 Why High Performance Permanent Magnets are Important . . . . .	1
<b>2 Magnetism and Magnetic Materials</b>	<b>3</b>
2.1 Introduction . . . . .	3
2.2 Magnetically Ordered Systems . . . . .	3
2.2.1 The Exchange Interaction . . . . .	3
2.2.2 Anisotropy . . . . .	3
2.2.3 Magnetic Domains . . . . .	3
2.2.4 Hysteresis . . . . .	4
2.2.5 The Demagnetizing Field . . . . .	4
2.2.6 Magnetic Materials . . . . .	4
<b>3 Exchange Coupled Nanocomposites</b>	<b>6</b>
3.1 Theoretical Considerations . . . . .	6
3.2 State of the Art . . . . .	6
<b>4 Experimental Methods and Methodology</b>	<b>9</b>
4.1 Synthesis Methods . . . . .	9
4.1.1 The Arc Furnace . . . . .	9
4.1.2 The Induction Furnace . . . . .	9
4.1.3 Spark Plasma Sintering (SPS) . . . . .	9
4.1.4 Mechanical Milling/Alloying (MM/MA) . . . . .	10
4.1.5 The Turbula Mixer . . . . .	10
4.1.6 Heat Treatment . . . . .	11

4.2	Structure and Microstructure Measurements . . . . .	11
4.2.1	X-Ray Diffraction (XRD) . . . . .	11
4.2.2	Scanning Electron Microscopy . . . . .	11
4.3	Magnetic Property Analysis, Equipment and Methodology . . . . .	11
4.3.1	Equipment . . . . .	11
4.3.2	Methodology . . . . .	11
4.3.3	First Order Reversal Curves (FORC) . . . . .	12
4.4	General Sample Synthesis . . . . .	13
4.4.1	Nd <sub>2</sub> Fe <sub>14</sub> B + 10 wt% $\alpha$ -Fe nanocomposites . . . . .	13
4.4.2	SmCo <sub>5</sub> + 20 wt% $\alpha$ -Fe nanocomposites . . . . .	13
<b>5</b>	<b>Effect of Short Time Annealing on The Interphase Exchange Coupling in Hard-Soft Magnetic Nanocomposites</b>	<b>14</b>
5.1	Nd <sub>2</sub> Fe <sub>14</sub> B + 10 wt% Fe nanocomposite powders . . . . .	14
5.1.1	Synthesis . . . . .	14
5.1.2	Structural and Microstructural Studies . . . . .	14
5.1.3	Magnetic Properties of Nd <sub>2</sub> Fe <sub>14</sub> B + 10 wt%Fe nanocomposites . . . . .	16
5.2	SmCo <sub>5</sub> + 20 wt% Fe magnetic nanocomposite powders . . . . .	16
5.2.1	Synthesis . . . . .	16
5.2.2	Structural and Microstructural Studies . . . . .	18
5.2.3	Magnetic Properties of SmCo <sub>5</sub> + 20 wt%Fe nanocomposites . . . . .	18
5.3	Partial Conclusions . . . . .	19
<b>6</b>	<b>Effect of Starting Powder Mixture on the Interphase Exchange Coupling of Soft-Hard Magnetic Nanocomposites Obtained by Mechanical Milling</b>	<b>21</b>
6.1	Effect of Hardness Disparity Within the Starting Powder . . . . .	21
6.1.1	Synthesis . . . . .	21
6.1.2	Structural and Microstructural Studies . . . . .	22
6.1.3	Magnetic Properties of Nd <sub>2</sub> Fe <sub>14</sub> B + 10 wt%Fe nanocomposites . . . . .	22
6.2	Effect of Phase Dispersal in Starting Powder Mixture on the Interphase Exchange Coupling in Hard-Soft Magnetic Nanocomposites . . . . .	26
6.2.1	Synthesis . . . . .	26
6.2.2	Structure and Microstructure Studies . . . . .	26
6.2.3	Magnetic Properties of Nd <sub>2</sub> Fe <sub>14</sub> B + 10 wt%Fe nanocomposites . . . . .	26
6.3	Partial Conclusions . . . . .	27

<b>7</b>	<b>Effect of Milling Energy on the Microstructure and Hard-Soft Exchange Coupling in Nanocomposite Magnetic Materials Obtained Trough Mechanical Milling</b>	<b>30</b>
7.1	Synthesis . . . . .	30
7.2	Structure and Microstructure Studies . . . . .	31
7.3	Magnetic Properties of $\text{Nd}_2\text{Fe}_{14}\text{B} + 10 \text{ wt}\% \text{Fe}$ nanocomposites obtained by different milling energy. . . . .	31
7.4	Partial Conclusions . . . . .	34
<b>8</b>	<b>Effect of Spark Plasma Sintering on Hard-Soft Interphase Exchange Coupling in Magnetic Nanocomposite Powders</b>	<b>35</b>
8.1	SPS Magnets Based on $\text{Nd}_2\text{Fe}_{14}\text{B} + 10\% \text{ Fe}$ Nanocomposites . . . . .	35
8.1.1	Synthesis . . . . .	35
8.1.2	Structural and Microstructural Studies . . . . .	35
8.1.3	Magnetic Properties of $\text{Nd}_2\text{Fe}_{14}\text{B} + 10 \text{ wt}\% \text{Fe}$ SPS nanocomposites . . . . .	36
8.2	SPS Magnets based on $\text{SmCo}_5 + 20 \text{ wt}\% \text{ Fe}$ Nanocomposites . . . . .	37
8.2.1	Synthesis . . . . .	37
8.2.2	Structural and Microstructural Studies . . . . .	37
8.3	Magnetic Properties of $\text{SmCo}_5 + 20 \text{ wt}\% \text{Fe}$ SPS Compacts . . . . .	38
8.4	Partial Conclusions . . . . .	38
<b>9</b>	<b>Conclusions and Future Prospects</b>	<b>40</b>
	Publications . . . . .	43
	Presentations . . . . .	45
	References . . . . .	46

# List of Tables

6.1	Powder characteristics and premixing method for each of the three $\text{Nd}_2\text{Fe}_{14}\text{B}+10\text{wt}\%\text{Fe}$ starting powders . . . . .	26
7.1	Milling media used for each data set . . . . .	30
8.1	Synthesis details and density for $\text{SmCo}_5+20\text{wt}\% \alpha\text{-Fe}$ SPS compacts . . . . .	37

# List of Figures

5.1	Demagnetization curves (a,c,e) and $dM/dH$ vs $H$ plots (b, d, f) for $\text{Nd}_2\text{Fe}_{14}\text{B}$ + 10 wt% $\alpha$ -Fe 6 h MM and annealed (as indicated) nanocomposites . . . . .	15
5.2	Demagnetization curves (a,c,e) and $dM/dH$ vs $H$ plots (b, d, f) for $\text{Nd}_2\text{Fe}_{14}\text{B}$ + 10 wt% $\alpha$ -Fe 6 h MM and annealed (as indicated) nanocomposites . . . . .	17
5.3	Demagnetization curves (a) and $dM/dH$ vs $H$ plots (b) for $\text{SmCo}_5$ + 20 wt% $\alpha$ -Fe nanocomposites 6 h MM and annealed at 500 - 600 °C for 0.5 to 1.5 hours . . . . .	18
5.4	Demagnetization curves (a) and $dM/dH$ vs $H$ plots (b) for $\text{SmCo}_5$ + 20 wt% $\alpha$ -Fe nanocomposites 6 h MM and annealed at 700 - 820 °C for 1.5 min . . . . .	19
6.1	Demagnetization curves (a,c,e) and $dM/dH$ vs $H$ plots (b, d, f) for $\text{Nd}_2\text{Fe}_{14}\text{B}$ + 10 wt% MH-Fe nanocomposites 6 h MM and annealed (as indicated) . . . . .	23
6.2	Demagnetization curves (a,c,e) and $dM/dH$ vs $H$ plots (b, d, f) for $\text{Nd}_2\text{Fe}_{14}\text{B}$ + 10 wt% MH-Fe nanocomposites 8 h MM and annealed (as indicated) . . . . .	24
6.3	Demagnetization curves (a, c, e) and $dM/dH$ vs $H$ plots (b, d, f) for $\text{Nd}_2\text{Fe}_{14}\text{B}$ + 10 wt% Fe 6 h MM and annealed (as indicated) nanocomposites . . . . .	28
7.1	Demagnetization curves (a, c, e) and $dM/dH$ vs $H$ plots (b, d, f) for $\text{Nd}_2\text{Fe}_{14}\text{B}$ + 10 wt% 6 h MM and annealed (as indicated) nanocomposites . . . . .	32
8.1	Demagnetization curves (a) and $dM/dH$ vs $H$ plots (b) for $\text{Nd}_2\text{Fe}_{14}\text{B}$ + 10 wt% Fe SPS compacts sintered at 700, 750 and 800 °C . . . . .	36
8.2	Demagnetization curves (a) and $dM/dH$ vs $H$ plots (b) for $\text{SmCo}_5$ + 20 wt% Fe SPS compacts . . . . .	39

# Chapter 1

## Introduction

*keywords: exchange coupling, spring magnets, coercivity, mechanical milling, annealing, microstructure, spark plasma sintering*

### 1.1 Preamble

In this work we have set out to study the influence of the microstructure on the interphase exchange coupling in hard-soft magnetic nanocomposites obtained through mechanical milling. To this end we have altered the microstructure formation process at every stage of synthesis, by either changing the powder mixture, tuning the milling energy and applying various annealing or SPS routes.

This thesis was produced at Ioan Ursu Institute of Physics at the Faculty of Physics, Babeş-Bolyai University, Cluj-Napoca, Romania.

The work presented was done in conjunction with several institutions: Université Grenoble Alpes, CNRS, Institut Néel, Grenoble, France; Technical University of Cluj-Napoca, Romania and INCDTIM, Cluj-Napoca, Romania.

### 1.2 General Context

#### 1.2.1 Why High Performance Permanent Magnets are Important

Permanent magnets are ubiquitous in today's society, as they are used in a wide range of applications, from the simple windscreen wipers, locks and microphones, to the ubiquitous smart phones and laptops, to contenders in the clean energy market such as electric vehicles and wind turbines [1]. If one were to estimate the number of magnets an average person owns, that number would probably be in the hundreds [2].

The performance of rare-earth based magnets is hard to beat. Given the ubiquity of magnets in modern society they have become crucial, but concerns about tight rare-earth supplies from China and the huge fluctuations in rare-earth price in recent years have driven researchers to look for ways to minimize the quantity of rare-earth elements used for the production of high performance permanent magnets [3]. These factors stimulated intense efforts, so new research and development routes emerged [4, 5]: 1) the increase of usage efficiency; 2) recycling; 3) new lean or non-rare-earth containing magnets. The latter was addressed mainly in three directions: a) modifying the rare-earth magnets [6, 7], b) hard magnetic phases with low content or without rare-earth [8–12] and c) hard/soft magnetic nanocomposites coupled by interphase exchange interactions [6, 13–18]. The current work follows latter direction.

## Chapter 2

# Magnetism and Magnetic Materials

### 2.1 Introduction

### 2.2 Magnetically Ordered Systems

#### 2.2.1 The Exchange Interaction

Magnetically ordered systems are those in which a percentage of the total energy is dependent on the alignment of neighbouring magnetic moments. The short range interactions which lead the ordering of magnetic moments is called the exchange interaction. More broadly the exchange interaction is a spin dependent electrostatic energy of the same order of magnitude as the Colombian interaction.

#### 2.2.2 Anisotropy

For the uniaxial case (in the above example, when the magnetic moment lies along the  $c$  axis), in a simple first term expansion, the anisotropy energy can be written as:

$$E_a = K \sin^2(\theta) \quad (2.1)$$

where  $K$  is called the anisotropy constant, and  $\theta$  is the angle made between the magnetization direction and the  $c$  axis.

#### 2.2.3 Magnetic Domains

Pierre Weiss assumed that a large piece of a magnetic material is made up of smaller magnetic regions called magnetic domains. Inside the magnetic domain, the magnetic moments are all

aligned along the same direction, but, in order to minimise the magnetostatic energy, the direction of magnetization differs between domains [19]. The transition between magnetic domains is not abrupt, but gradual and their length is dictated both by the anisotropy energy and the exchange energy. These transition areas are called domain walls.

### 2.2.4 Hysteresis

A system which presents hysteresis is a system in which the final state of the system depends on the system's history, i.e. all the intermediate states which lead up to the final state. In other words, the transformations suffered by the system are not reversible.

We introduce the saturation magnetization  $M_s$  which is the maximum magnetization, all the magnetic domains are parallel aligned. The remanent magnetization  $M_r$  which is the value of the magnetization which remains after the external field has been removed. The coercive field  $H_c$  which is the value of the opposite applied magnetic field, required to bring the moment back to zero after the material was saturated.

The energy product  $(BH)_{max}$  represents the maximum energy which can be stored in a magnetic material.

### 2.2.5 The Demagnetizing Field

The free magnetic poles which appear at the surface of magnetic materials give rise to a magnetic field  $H_d$  in the opposite direction to the magnetization, this field is called the demagnetizing field:

$$H_d = -N_d M \quad (2.2)$$

where  $N_d$  is called the demagnetizing factor.

### 2.2.6 Magnetic Materials

Though magnetic materials can be classified in many ways, for the purposes of this study we would like to put forward the classification into soft and hard magnetic materials. This classification is based on the value of the coercive field of a material. Low values means the material is soft i.e. the direction of the magnetization is easily changed, while hard means that the material resists the external field (it has a high value of the coercive field).

#### Soft Magnetic Materials

In this subsection we would like to focus specifically on the soft  $\alpha$ -Fe phase and the effect of Co addition on its magnetic properties. Fe is the most abundant metal in the known universe. From

room temperature up to 1185 K it has a Body centred cubic (BCC) structure and is ferromagnetic up to its Curie temperature of 1044 K.

### **Hard Magnetic Materials**

Hard magnetic materials are characterized by high anisotropy and high coercivity. The most competitive hard magnetic materials currently available are based on rare earth metals such as Sm and Nd.

## Chapter 3

# Exchange Coupled Nanocomposites

### 3.1 Theoretical Considerations

The idea of hard-soft exchange coupled nanocomposite magnets, otherwise known as spring magnets was first proposed by Kneller and Hawing [15]. The basic premise of the spring magnet comes from the idea that we could obtain a magnetic material with a high energy product by combining a material which has a high magnetization (a soft magnetic phase) with a material which has a high magnetocrystalline anisotropy (a hard magnetic phase). The hard magnetic material is meant to stiffen the magnetic structure of the soft magnetic material. This was proposed as being achievable in a composite nanomaterial.

### 3.2 State of the Art

Even if exchange coupled nanocomposites show a lot of promise, researchers still struggle with the synthesis of these kinds of materials, especially with the optimization of the microstructure required to make these types of materials feasible.

Theoretical calculations highlight the importance of the microstructure. The geometry of the grains is pivotal, the difference in energy product between embedded layers, cylindrical inclusions and core shell type particles proving to be drastically different [22–25].

It was also calculated that large energy products can be attained even for soft phase volume fractions of 80% [25]. On the other hand the choice of the soft phase also plays an important role with respect to the properties of exchange coupled hard-soft nanocomposites. While phases such as  $\text{Fe}_{65}\text{Co}_{35}$  lead to high energy products, others such as Co are predicted to allow for larger soft phase grains thus lessening the synthesis constraints [26–28].

While the choice of the soft phase is of great import, as mentioned previously, the general microstructure of the composite determines the final magnetic properties of the nanocomposite

and therefore the effect of irregular grains was investigated using micromagnetic simulations, and it was found that grain sizes should not exceed 20 nm for the hard magnetic phase ( $\text{Nd}_2\text{Fe}_{14}\text{B}$ ) and 10 nm for the soft magnetic phase ( $\alpha\text{-Fe}$ ) in order to obtain a good degree of interphase exchange coupling [29, 30]. Additionally the matter of microstructure optimization is further complicated due to the fact that even if grain sizes are kept in check, easy axis misalignment can lead to reductions in the energy product [31]. Moreover it has been shown that at the interface between hard and soft grains (in the specific case of  $\text{Nd}_2\text{Fe}_{14}\text{B} + \alpha\text{-Fe}$ ) the short Fe - Fe distances lead to antiferromagnetic coupling, a case which does not hold up for Co [32], this was also confirmed experimentally in thin films [33] but has not been observed yet in bulk materials.

Experimental studies have explored a great deal of synthesis routes in the attempt of creating exchange coupled nanocomposites with good properties i.e. well designed microstructures and high energy products, such as : melt-spinning [34], mechanical milling [35], sono chemical synthesis [36], bulk injection casting [37], suction casting [38], hot deformation [39], thin films [40] etc.

In the hopes of improving the magnetic properties of hard-soft nanocomposites, researchers have also tried doping the hard and soft phases with various elements such as: Ti [41], Dy [42], Co, Zr, Ga [43, 44], Gd [45] or Cr and Cu [46].

While the energy products obtained so far remain relatively low, some of the benefits of exchange coupled hard-soft magnetic nanocomposites predicted by Kneller and Hawig [15] were attained in practice such as the improved temperature stability [47] [48], corrosion resistance and surface passivation [49].

Even though very good experimental results have been reported in epitaxial  $\text{SmCo}_5/\text{Fe}$  multilayers with energy products of over  $400 \text{ kJ/m}^3$  [50], in general the energy products obtained so far are not at the level of theoretical prediction because the optimization of the microstructure for exchange coupled hard-soft magnetic nanocomposites has proven to be very difficult especially in compacts. The effects of these uneven microstructures are not necessarily immediately obvious from the normal demagnetization or hysteresis curves, but can be better visualised in FORC data [41, 51]. Moreover it was shown that the structures resulting in bulk (in this case specifically, annealed amorphous ribbons of  $\text{Nd}_2\text{Fe}_{14}\text{B}$ ) tend to form a structure of embedded hard grains. This is due to the fact that when the hard phase recrystallizes it pushes the additional material (the soft phase) to the grain boundary [52]. For  $\text{Nd}_2\text{Fe}_{14}\text{B} + \alpha\text{-Fe}$  this mechanism favours the formation of fairly consistent chemical compositions for both the soft and hard magnetic phase, while in the case of  $\text{SmCo}_5 + \alpha\text{-Fe}$  mass transfer between the two phases can occur, resulting in exchange coupled nanocomposites in which the hard phase is doped with Fe and the soft phase is doped with Co [53].

In the case of a composite material formed out of three phases: hard, semi-hard and soft, it was shown that the semi-hard phase can act as a nucleation site for the hard phase. In the case of

mechanically milled samples, defect regions can act in the same way. The defect regions appear due to the milling process and can reduce the coercivity of the final nanocomposites, because they have a lower anisotropy than the perfect hard phase regions. Since the defect regions are exchange coupled to both hard and soft regions, the domain wall energy in the soft phase needs only equal the wall energy in the defect region in order to invade it, which leads to the easy nucleation of the remaining perfect hard phase regions [54]. This problem is made worse by the fact that the synthesis of exchange coupled hard-soft magnetic nanocomposites through mechanical milling requires large shock energies which lead to the creation of many defects [55].

In most cases, the route of synthesis starts with the creation of an amorphous or nanocrystalline composition such as amorphous ribbons or powders [16, 56] or even a combination of the two i.e. powders created by milling amorphous ribbons [57]. This step is usually followed by short annealing or sintering in spark plasma sintering equipments [58].

In the scientific literature, researchers have used a very large variety of synthesis methods in the attempt to produce exchange coupled hard-soft magnetic nanocomposites, each with slightly differing results [37][56][59][36][28]. We have decided, in this work, to go down a single synthesis route and investigate the influence that each step of the process has on the final magnetic properties of the materials produced. To this end we have selected mechanical milling, due to the accessibility and scalability of the method, for the production of the nanocrystalline or amorphous composite material which is followed by annealing, SPS or both. We have proposed to study this synthesis route at all stages from the influence of the starting powder mixture, to the energies and mechanisms involved in the milling process to the optimization of the annealing and sintering processes. The aim is to point out the areas in the overall process where additional research is best directed and to provide a starting point for future studies by investigating the physical processes which most influence the properties of the final material.

## Chapter 4

# Experimental Methods and Methodology

### 4.1 Synthesis Methods

#### 4.1.1 The Arc Furnace

The arc furnace is a very wide spread synthesis method for polycrystalline materials [60]. The furnace works by creating an electric arc between the tungsten tip and the surface of the sample. The arc furnace can reach temperatures of over 2000 °C. Because the heating mechanism is based on electric conductivity this method is not suitable for all materials. At least one constituent of the alloy must be a conductor [61].

#### 4.1.2 The Induction Furnace

The induction furnace heats up metallic samples by applying a high frequency (HF) electromagnetic field. Of course, since the method of heating is fundamentally the Joule effect (like in the case of the arc furnace Section 4.1.1) at least one of the sample components must be conductive.

#### 4.1.3 Spark Plasma Sintering (SPS)

Sintering is a technological process through which materials may be produced using powder metallurgy i.e. powdered materials may be densified into bulk materials through the application of heat. The aim is to achieve mass transfer inside pressed powder compacts by the application of thermal energy, thus filling the inter particle voids and reducing the volume of the compact, thus increasing its density.

In Spark Plasma Sintering (SPS) the heating process is driven by the application of large currents via graphite electrodes to the powder compact. The electric discharge dissipates a large amount of energy within the powder which translates to a very high and homogeneous heating rate. Pressure is applied during the process in order to favour densification.

#### **4.1.4 Mechanical Milling/Alloying (MM/MA)**

Mechanical milling/Alloying is a powder processing technique which involves the synthesis of various materials through repeated fracturing and re-welding processes, inside a high energy ball mill.

##### **Milling Machines**

There are several types of mill designs, such as vibratory mills (shaker mills), planetary ball mills, attritor mills, etc [62, 63]. In this work we will only discuss planetary ball mills.

##### **Process Description**

The milling process consists of a succession of fracturing and welding processes which occur when powder particles are trapped between balls (or between a ball and the inner wall of the vial), as depicted by E. Gaffet in [62]. This means that some mass transfer between powder particles is inevitable.

##### **Milling Machine Modeling, The Planetary Ball Mill**

Mechanical milling is a very difficult process to describe analytically, in part due to the large number of bodies traveling at high speeds inside the vial. Analytic models can approximate the total power of the milling process, but can not accurately assess how much of it is transferred to the powder. This is due to the fact that it is difficult to calculate the impact frequency and impact angle of a ball. However, such information can be obtained through computer simulation [64–66].

#### **4.1.5 The Turbula Mixer**

The Turbula mixer is a device used for mixing powders or liquids. The special movement generated by the Schatz linkage (more commonly known as the Turbula linkage) [67] prevents particle segregation according to mass and size. From the list of features of this mixer design we would also like to highlight the fact that mixing can be done in sealed containers, under controlled atmosphere (in our case high purity Ar gas). This is very important when working with materials containing rare-earth metals as they oxidize easily.

### 4.1.6 Heat Treatment

In this work, heat treatment has two functions. The first is to stabilize and homogenize the magnetic phases in the ingots used as the starting samples for the milling process. And the second is to recrystallize the desired phases from the amorphous as-milled powders.

## 4.2 Structure and Microstructure Measurements

### 4.2.1 X-Ray Diffraction (XRD)

X-Ray diffraction (XRD) is used for phase identification, and for determining the average grain sizes for each phase, post milling and annealing.

Phase identification is done for the master alloys and for the final powders.

The average crystallite sizes are measured using the Scherer equation [68]:

$$D = \frac{K\lambda}{\beta \cos(\theta)} \quad (4.1)$$

where  $D$  is the average crystallite size,  $K$  is a dimensionless shape factor,  $\lambda$  is the wavelength of the X-rays,  $\beta$  is the full width at half maximum of the peak (FWHM) minus the instrumental broadening and  $\theta$  is the Bragg angle.

### 4.2.2 Scanning Electron Microscopy

Scanning electron microscopes (SEM) were used for the determination of the shape and size of the powder particles and the crystallite sizes in the nanocomposite powders, through imaging. The SEM was also used to check the chemical composition and dispersal of the chemical elements in the nanocomposite. This was done by energy dispersive X-Ray spectroscopy (EDXS), i.e. by analysing the specific X-ray radiation emitted by the atoms which make up our samples.

## 4.3 Magnetic Property Analysis, Equipment and Methodology

### 4.3.1 Equipment

The magnetic properties of the samples discussed in this work were measured using the extraction or the vibrating sample method.

### 4.3.2 Methodology

In order to block the powder particles, ensuring an accurate measurement, they were encapsulated in epoxy resin. Moreover as the samples contain rare-earths the resin also provides some

resistance against oxidation. The demagnetizing factor  $N_d$  for these samples was taken to be 1/3, the same as for isolated spheres (this approximation was considered viable because the volumetric resin to powder ratio is very large). For sintered samples, whole pieces were used, and the demagnetizing factor was calculated assuming they are of square cross-section [20]. These calculations allow us to approximate the internal field  $H_{int} = H_{appl} - N_d M$ .

All samples were studied by demagnetization curves and their derivative with respect to the applied field. The demagnetization curves are used for the estimation of the coercive field  $H_c$ , the remnant magnetization  $M_r$  and the maximum energy product  $(BH)_{max}$ . The derivative yields qualitative information about the interphase exchange coupling. Variations in the rate of domain reversals produce peaks in the  $dM/dH$  vs  $H$  plot. Therefore peaks at large fields are indicative of good exchange coupling, while peaks at low fields are indicative of poor interphase exchange coupling. The relative intensity of the high field (HF) and low field (LF) peaks also yields qualitative information. Samples with a higher ration of HF/LF peak intensities present better interphase exchange coupling.

All magnetic measurements in this work were recorded at 300 K.

### 4.3.3 First Order Reversal Curves (FORC)

#### The Preisach Model Of Magnetism

I.D. Mayergoz defines hysteresis as " a nonlinearity with a memory which reaveals itself trough branching " [69]. This general definition also serves to highlight the fact that hysteresis phenomenon can be encountered in many fields besides magnetism (such as ferroelectric hysteresis, mechanical hysteresis, electron beam hysteresis etc.), nevertheless the general mathematical treatment of hysteresis can be applied to any of them.

#### The Classical Preisach Model of Hysteresis

In order to adequately describe this model we first must introduce the simplest hysteresis operator which consists of a single rectangular loop.

This loop can only have two output states (magnetic moment in our case),  $\Delta m$  and  $-\Delta m$ . The input values (applied field)  $\alpha$  and  $\beta$  correspond to the switching values between the 2 outputs i.e. when  $H$  exceeds the value  $\alpha$  the moment is switched to  $\Delta m$  and when the field is swept below  $\beta$  the output switches to  $-\Delta m$ , otherwise it remains at its previous value. Obviously what we have described above is a system with local memory. In practice, in magnetism, we deal with system of greater complexity with non-local memory. However by taking our basic model and we can expand it by saying that our real-life systems can be represented trough a superposition of many such simple rectangular loops. Therefore, we model reality by considering that every magnetic domain contained in our material can be represented by one of these simple rectangular hysteresis

loops. Of course in order to accurately model a magnetic hysteresis loop, we must introduce a function  $n(h_c, h_u)$ . Here  $h_c$  and  $h_u$  are defined in terms of  $\alpha$  and  $\beta$  (Equations 4.2).

$$\alpha = h_u + h_c \text{ and } \beta = h_u - h_c \quad (4.2)$$

The magnetization of the system is the contribution from of all units in the distribution [70] :

$$\int_0^\infty dhc \int_{-\infty}^\infty n(h_c, h_u) dh_u = N \quad (4.3)$$

where  $n(h_c, h_u) dh_c dh_u$  represents the number of units in element  $dh_c dh_u$

### First Order Reversal Curves

The FORC method allows us to investigate the Preisach distribution of a sample experimentally.

$$p(h_c, h_u) = -\frac{\partial M(h_c, h_u)}{\partial h_c \partial h_u} \quad (4.4)$$

## 4.4 General Sample Synthesis

### 4.4.1 Nd<sub>2</sub>Fe<sub>14</sub>B + 10 wt% $\alpha$ -Fe nanocomposites

In general the Nd<sub>2</sub>Fe<sub>14</sub>B ingot is obtained by first arc melting a Fe<sub>14</sub>B ingot, remelting it alongside the required amount of Nd in an induction furnace and then annealing the resulting material at 950 °C for 72 h. This process ensures that the ingot is homogeneous and hence once crushed, Nd<sub>2</sub>Fe<sub>14</sub>B powder used for milling is homogeneous as well. After crushing, the Nd<sub>2</sub>Fe<sub>14</sub>B powder is sieved through a sieve with an opening of 500  $\mu$ m and the resulting powder is mixed with 10 wt% Fe powder. The mixture is then milled in a planetary ball mill (Frisch Pulverisete 4) under high purity Ar gas. The milling vials (80 ml) and balls are made of 440C hardened steel. The ratio between the rotation speed of the disc and the relative rotation speed of the vials was  $\Omega/\omega = 333/900$  rpm with a ball-to-powder weight ratio of 10:1.

### 4.4.2 SmCo<sub>5</sub> + 20 wt% $\alpha$ -Fe nanocomposites

The SmCo<sub>5</sub> phase was obtained by induction melting of the stichiometric quantities of Sm and Co and subsequent annealing at 950 °C for 72 h. The resulting ingot is then crushed (powder particles < 500  $\mu$ m) and mixed with Fe powder (particle size < 100  $\mu$ m) in a 80 to 20 % weight ratio respectively. The powder mixture was milled in a planetary ball mill (Frisch Pulverisete 4) for 6 h. The milling vials (80 ml) and balls (10 mm in diameter) are made of 440C hardened steel. The ratio between the rotation speed of the disc and the relative rotation speed of the vials was  $\Omega/\omega = 333/900$  rpm with a ball-to-powder weight ratio of 10:1.

## Chapter 5

# Effect of Short Time Annealing on The Interphase Exchange Coupling in Hard-Soft Magnetic Nanocomposites

### 5.1 Nd<sub>2</sub>Fe<sub>14</sub>B + 10 wt% Fe nanocomposite powders

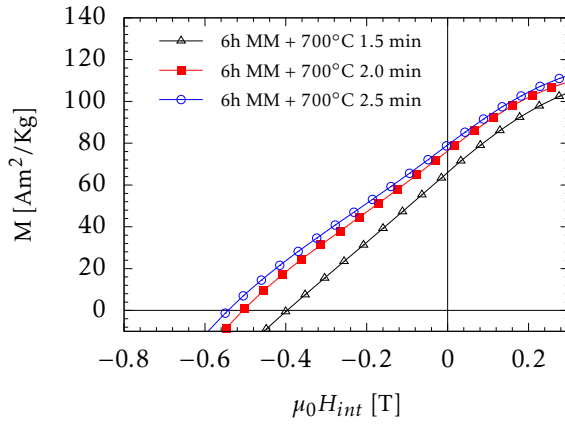
#### 5.1.1 Synthesis

We prepared Nd<sub>2</sub>Fe<sub>14</sub>B + 10 wt%  $\alpha$ -Fe nanocomposite powders in the manner described in Section 4.4.1, using  $\alpha$ -Fe powder with particle sizes < 100  $\mu$ m. The powder mixture was milled for 6 and 8 h using  $\varnothing = 10$  mm balls.

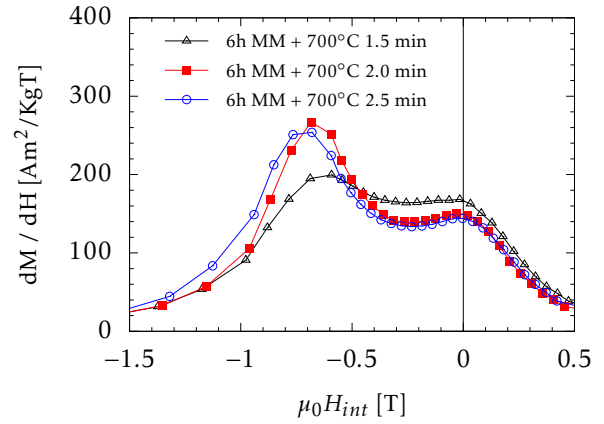
#### 5.1.2 Structural and Microstructural Studies

Milling destroys the crystallinity of the hard magnetic phase. By annealing for a short duration at temperatures between 700 and 800 °C (above the recrystallization temperature of the Nd<sub>2</sub>Fe<sub>14</sub>B [16]) the characteristic peaks of the hard magnetic phase reappears in the XRD patterns for both 6 h MM and 8 h MM sample sets.

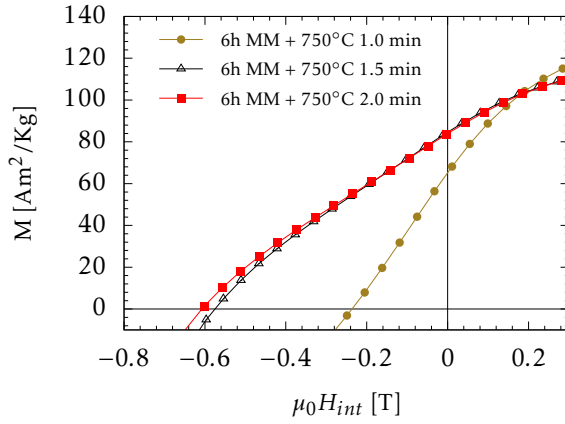
The average size of the soft phase grains for the 6 h MM annealed samples are larger than those of the 8 h MM ones. However, after annealing these values remain in the 5-20 nm range meaning that the excessive growth of the soft phase crystallites was hampered during the short time annealing.



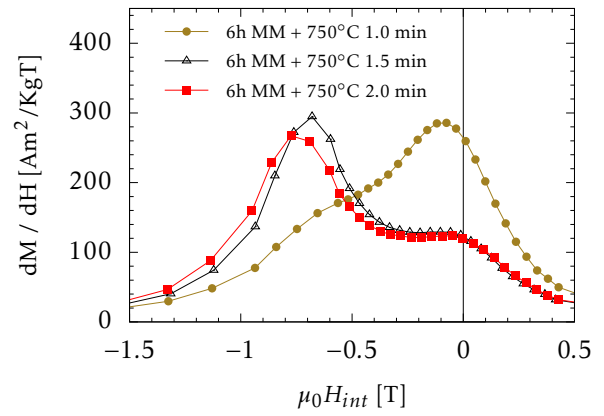
(a) Annealed at 700 °C for 1.5, 2 and 2.5 min



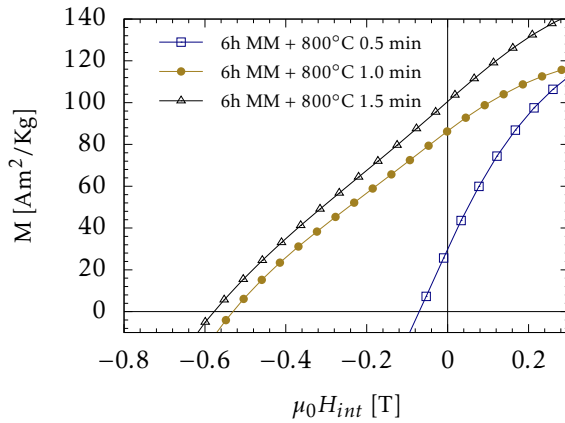
(b) Annealed at 700 °C for 1.5, 2 and 2.5 min



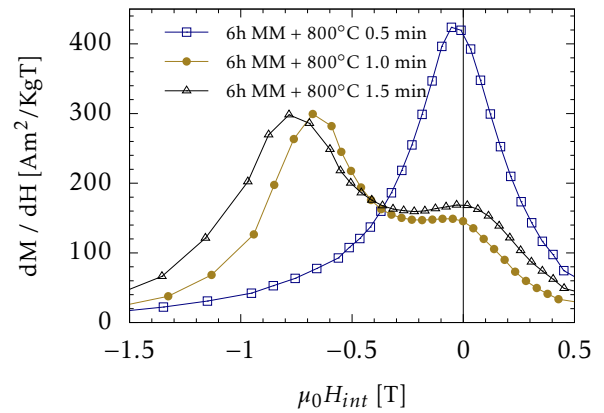
(c) Annealed at 750 °C for 1, 1.5 and 2 min



(d) Annealed at 750 °C for 1, 1.5 and 2 min



(e) Annealed at 800 °C for 0.5, 1 and 1.5 min



(f) Annealed at 800 °C for 0.5, 1 and 1.5 min

Figure 5.1: Demagnetization curves (a,c,e) and  $dM/dH$  vs  $H$  plots (b, d, f) for  $\text{Nd}_2\text{Fe}_{14}\text{B} + 10 \text{ wt}\% \alpha\text{-Fe}$  6 h MM and annealed (as indicated) nanocomposites

### 5.1.3 Magnetic Properties of $\text{Nd}_2\text{Fe}_{14}\text{B} + 10 \text{ wt}\% \text{Fe}$ nanocomposites

Magnetic measurements show that the magnetic properties of the investigated samples are highly dependent on both annealing time and temperature. The demagnetization curves show that, for used interval of time and temperature, both remanence and coercivity values improve by increasing the annealing temperature and time. These improvements are seen for both 6 h and 8 h milled nanocomposites. Due to the fact that the 8 h MM samples present a greater defect density, they generally exhibit lower values of  $M_r$  and  $H_c$  than the samples which were milled for 6 h.

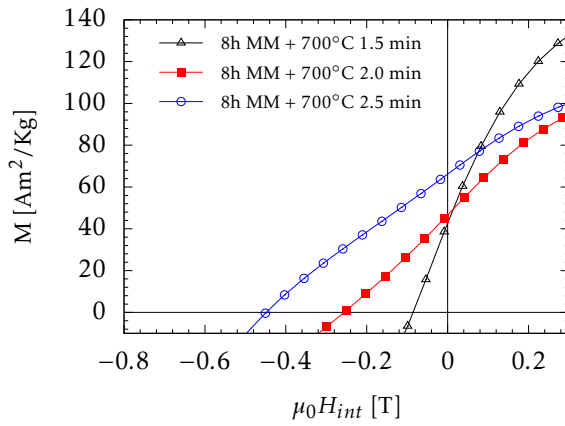
The relationship between the magnetic properties of the samples and annealing temperature is clearly pointed out when we look at the samples annealed for 1.5 min. We see that in the case of the 6 h MM samples the values of  $H_c$  and  $M_r$  improve with temperature leading to a more than two fold increase in the energy product  $(BH)_{max}$  from 30 to 57 to 70  $\text{KJ/m}^3$  over a temperature interval of 100 °C. The trend is also seen in the 8 h MM samples, however the increase in energy product when going from 700 to 750 °C is an entire order of magnitude (from 4 to 40  $\text{KJ/m}^3$ ) while further increase in temperature only leads to an improvement of 5%. This difference between the 6 h MM and 8 h MM samples reinforces the idea that even though increased milling time leads to lower  $\alpha$ -Fe phase grain sizes the additional damage to the  $\text{Nd}_2\text{Fe}_{14}\text{B}$  structure is significant, a fact especially visible for the samples annealed at 700 °C for 1.5 min where the increase in milling time leads to a drop in  $(BH)_{max}$  from 30 to 4  $\text{KJ/m}^3$  a nearly eight fold decrease.

The effectiveness of the interphase exchange coupling was studied using  $dM/dH$  vs  $H$  plots (See section 4.3.2). We can see that the ration between well coupled and poorly coupled particles increases by increasing annealing temperature. This is best exemplified when looking at the set of samples made up of those annealed for 1.5 min where we can see that the irreversible peak shifts to higher field values as annealing temperature is increased for both 6 h MM and 8 h MM samples, Figures 5.1 and 5.2. When we look in the same manner at the samples which were milled for 8 h (Figures 5.2b, 5.2d, 5.2f) we see that each data set contains at least one sample for which the nucleation behavior is dictated by the soft magnetic phase i.e. we see only a large peak at low field, but again we see that by slightly increasing the annealing time, the irreversible peak reappears.

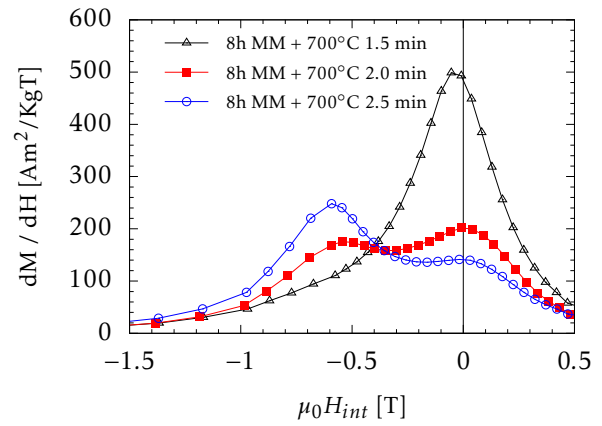
## 5.2 $\text{SmCo}_5 + 20 \text{ wt}\% \text{Fe}$ magnetic nanocomposite powders

### 5.2.1 Synthesis

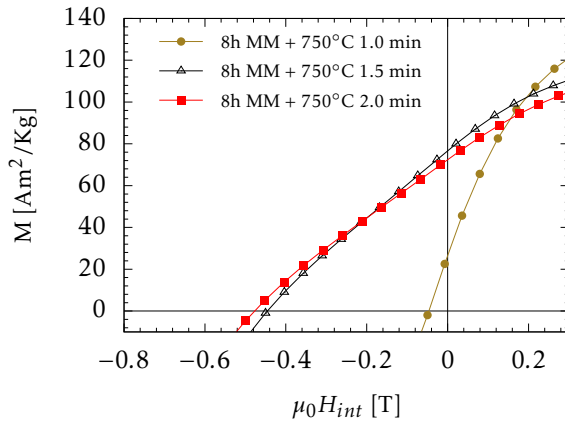
The  $\text{SmCo}_5 + 20\text{wt}\% \alpha\text{-Fe}$  nanocomposite samples were prepared in the manner described in Section 4.4.2, followed by annealing at temperatures between 500 and 820 °C.



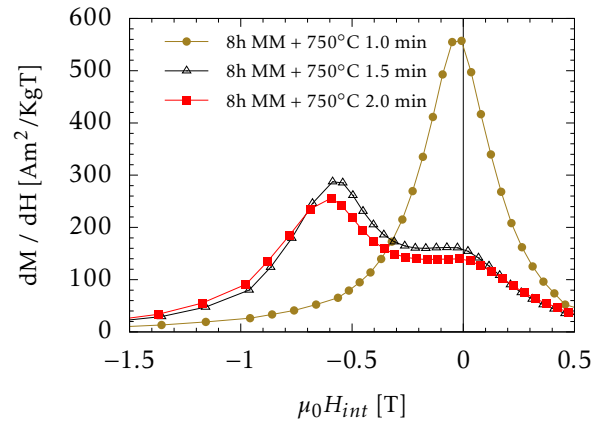
(a) Annealed at 700 °C for 1.5, 2 and 2.5 min



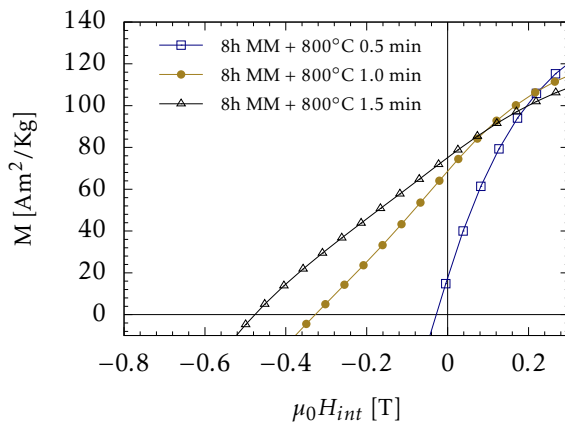
(b) Annealed at 700 °C for 1.5, 2 and 2.5 min



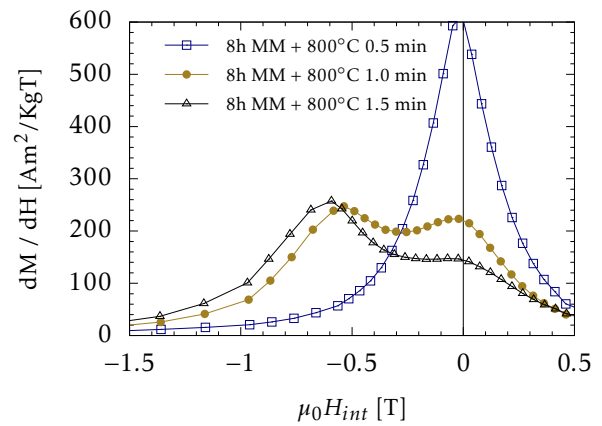
(c) Annealed at 750 °C for 1, 1.5 and 2 min



(d) Annealed at 750 °C for 1, 1.5 and 2 min



(e) Annealed at 800 °C for 0.5, 1 and 1.5 min



(f) Annealed at 800 °C for 0.5, 1 and 1.5 min

Figure 5.2: Demagnetization curves (a,c,e) and  $dM/dH$  vs  $H$  plots (b, d, f) for  $\text{Nd}_2\text{Fe}_{14}\text{B} + 10 \text{ wt}\% \alpha\text{-Fe}$  6 h MM and annealed (as indicated) nanocomposites

### 5.2.2 Structural and Microstructural Studies

XRD patterns were recorded for both classically annealed and rapidly annealed samples. Both classical and rapid annealing regimes have proven effective in the recovery of the hard magnetic phase with the peaks attributed to the  $\text{SmCo}_5$  and  $\alpha\text{-Fe}$  phases being clearly visible. Moreover the peaks attributed to the hard magnetic phase become better resolved with increasing temperature for both types of heat treatment.

In both cases the average crystallite sizes were also estimated using the Scherrer method (Equation 4.1). We can see that for the classical annealing, raising the temperature from 500 to 550 °C produces a large increase in the average crystallite sizes for  $\alpha\text{-Fe}$ , but only a small increase in the case of the  $\text{SmCo}_5$  phase. However further increasing the annealing temperature while lowering the duration (from 1.5 h at 550 °C to 0.5 h at 600 °C), the microstructure can be kept in check.

For short time annealing, crystallite sizes vary linearly with annealing temperature. Fe crystallite sizes are kept in the 5 - 20 nm range.

### 5.2.3 Magnetic Properties of $\text{SmCo}_5 + 20 \text{ wt}\% \alpha\text{-Fe}$ nanocomposites

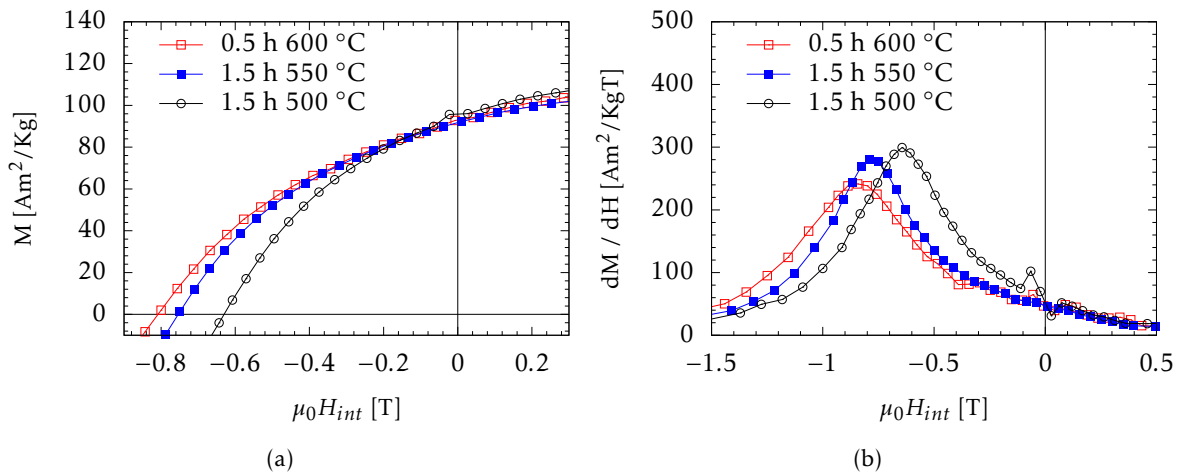


Figure 5.3: Demagnetization curves (a) and  $dM/dH$  vs  $H$  plots (b) for  $\text{SmCo}_5 + 20 \text{ wt}\% \alpha\text{-Fe}$  nanocomposites 6 h MM and annealed at 500 - 600 °C for 0.5 to 1.5 hours

The magnetic properties for both data sets, classical and short time annealing respectively, were investigated through demagnetization curves and  $dM/dH$  vs  $H$  plots (see Section 4.3.2). From the demagnetization curves (Figures 5.3a and 5.4a) we can see that for the classical annealed samples, remanence remains the same for all samples, while  $H_c$  increases with temperature. The same trend is observed for the rapidly annealed samples, however in this case we also notice an improvement in the rectangularity of the curves with increasing annealing temperature. Moreover

this behaviour is confirmed by the derivative of the magnetization vs field (Figures 5.3b and 5.4b) where in the case of the classically annealed samples the high field maximum shifts to higher values with increased annealing temperature, while in the case of the rapidly annealed samples, the peaks not only shift to higher values but also become narrower at higher annealing temperature, which means that the majority of domain reversal phenomenon take place in a narrower band i.e the shape of the hysteresis curve becomes more rectangular.

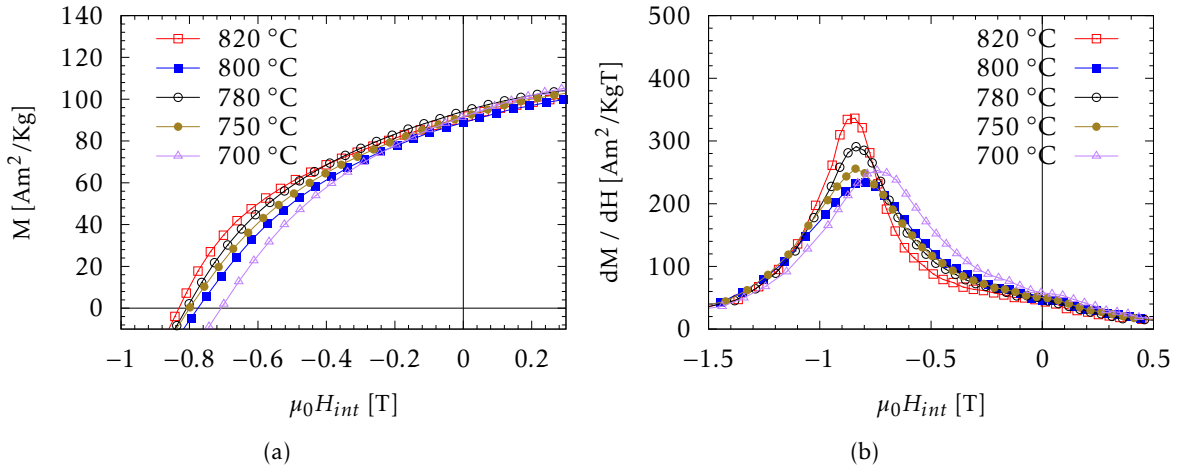


Figure 5.4: Demagnetization curves (a) and  $dM/dH$  vs  $H$  plots (b) for  $\text{SmCo}_5 + 20 \text{ wt\% } \alpha\text{-Fe}$  nanocomposites 6 h MM and annealed at 700 - 820 °C for 1.5 min

We see that even though we have a high variation in  $\alpha\text{-Fe}$  grains sizes. In the samples annealed at 500, 550 and 600 °C, the energy product varies only slightly from 91 to 98  $\text{KJ/m}^3$ . Of course this increase is associated with the increased coercivity from 0.63 T at 500 °C to 0.81 T at 600 °C and remanence (from 90 to 94  $\text{Am}^2/\text{Kg}$ ). The relatively small variations in  $(BH)_{max}$  is also observed in the samples annealed for 1.5 min, from 89  $\text{KJ/m}^3$  at 700 °C to the peak value of 103  $\text{KJ/m}^3$  at 780 °C. It should be noted that the best samples of each set have the same  $H_c$ , 0.81 T and the same  $M_r$ , of 94  $\text{Am}^2/\text{Kg}$ , but the sample annealed for 1.5 min has a 5% higher energy product, due to increased rectangularity of the demagnetization curves, despite the slightly higher  $\alpha\text{-Fe}$  grain sizes.

### 5.3 Partial Conclusions

In summary, for  $\text{Nd}_2\text{Fe}_{14}\text{B} + 10\% \alpha\text{-Fe}$  exchange coupled hard-soft magnetic nanocomposite samples obtained through mechanical milling, short time annealing has proven effective in restoring the crystallinity of the hard magnetic phase while also keeping the  $\alpha\text{-Fe}$  grain sizes low. This proves that it is a viable synthesis route for spring magnets in which a good degree of interphase exchange coupling can be achieved, reflected in the high  $H_c$  values of around 0.6 T and  $M_r$  of up to 100

$\text{Am}^2/\text{Kg}$ .

In the case of  $\text{SmCo}_5 + 20\% \text{Fe}$  nanocomposite samples obtained through mechanical milling, it was shown that both short time annealing and classical annealing lead to a good degree of inter-phase exchange coupling. However, short time annealing at high temperatures lead to improved rectangularity in the demagnetization curves and a 5% increase in the energy product. These results are encouraging with respect to the transferral of such annealing regimes to an SPS synthesis route where higher temperatures also lead to higher sample densities.

## Chapter 6

# Effect of Starting Powder Mixture on the Interphase Exchange Coupling of Soft-Hard Magnetic Nanocomposites Obtained by Mechanical Milling

### 6.1 Effect of Hardness Disparity Within the Starting Powder

#### 6.1.1 Synthesis

In order to study the effect of  $\alpha$ -Fe particle size reduction in the starting mixture on the interphase exchange coupling in  $\text{Nd}_2\text{Fe}_{14}\text{B} + \alpha\text{-Fe}$  nanocomposites, the soft magnetic phase was pre-milled for 4 h. However this process lead to a significant increase in the mechanical hardness of the  $\alpha$ -Fe phase. Therefore the focus of the study was widened to include the investigation of the effect of the mechanical hardness disparity between the  $\alpha$ -Fe and  $\text{Nd}_2\text{Fe}_{14}\text{B}$  phases in the starting mixture. To this end we prepared 6 h and 8 h milled  $\text{Nd}_2\text{Fe}_{14}\text{B} + \alpha\text{-Fe}$  nanocomposites (in the manner described in Section 4.4.1, using  $\varnothing = 10$  mm balls) with 4 h dry-milled Fe powder as the low anisotropy phase. The mechanical hardness of the pre-milled Fe powder (MH-Fe) was measured by nanoindentation to be 840 MPa, significantly higher than 670 MPa for the un-milled  $\alpha$ -Fe used in the previous Chapter 5 (a value similar to that for  $\text{Nd}_2\text{Fe}_{14}\text{B}$ ).

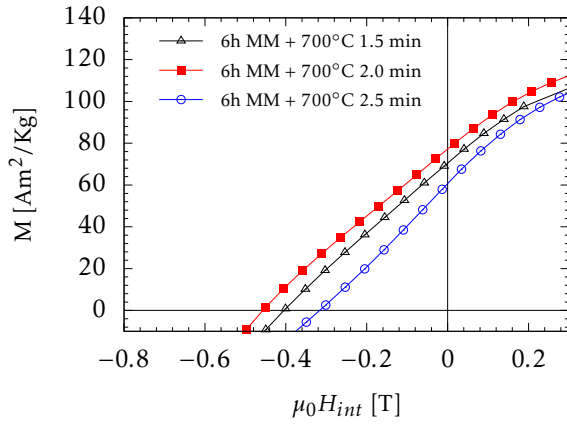
### 6.1.2 Structural and Microstructural Studies

The average crystallite sizes for the soft magnetic phase were measured in this case as well. The results are comparable with those recorded in the case of unhardened iron.

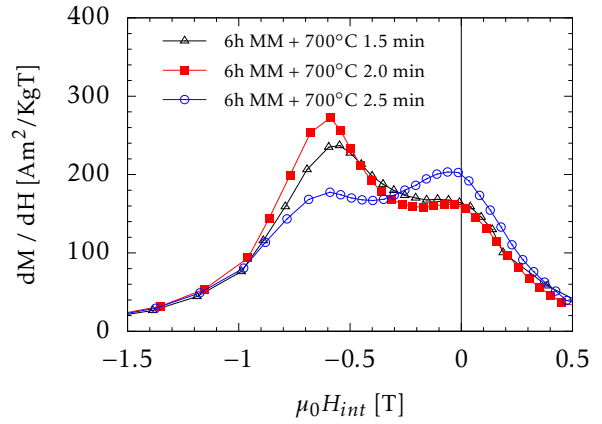
### 6.1.3 Magnetic Properties of $\text{Nd}_2\text{Fe}_{14}\text{B} + 10 \text{ wt}\% \text{Fe}$ nanocomposites

For the  $\text{Nd}_2\text{Fe}_{14}\text{B} + 10 \text{ wt}\% \text{MH-Fe}$  we see a maximum coercive field of 0.53 T, a lower value than for the samples made with unhardened  $\alpha\text{-Fe}$  of 0.61 T. The use of MH-Fe produces samples with lower  $H_c$  and  $M_r$  compared to the values obtained for samples with unhardened Fe, described in section 5.1. Moreover, if we look at the energy product of the samples we see that the maximum values are  $50 \text{ KJ/m}^3$  and  $41 \text{ KJ/m}^3$  for the 6 h MM and 8 h MM samples respectively. This represents a significant drop in  $(BH)_{max}$  for the 6 h MM samples, compared to the previous case, where the maximum value was  $70 \text{ KJ/m}^3$ . On the other hand, the best results for the 8 h MM samples, in terms of energy product are comparable  $42 \text{ KJ/m}^3$  versus  $41 \text{ KJ/m}^3$  for the samples made with  $\alpha\text{-Fe}$  and MH-Fe respectively. Once again we see that increasing the milling duration from 6 to 8 h, coercivity suffers greatly, often remaining under 0.1 T after annealing, this leads to very poor energy products (lower than  $10 \text{ KJ/m}^3$ ), due to the strong damage of the hard magnetic structure.

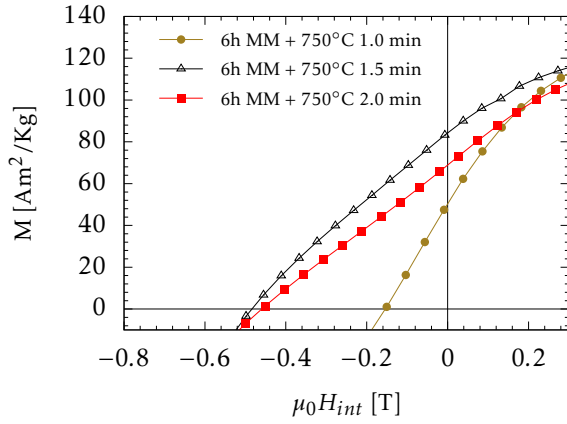
Some evidence for the delayed formation of the microstructure necessary for achieving a good degree of exchange coupling between the  $\text{Nd}_2\text{Fe}_{14}\text{B}$  and MH-Fe can be observed when we compare the magnetic properties of the samples milled for 6 h with those milled for 8 h. In the case of the 6 h MM samples annealed at  $700 \text{ }^\circ\text{C}$ , Figure 6.1a and 6.1b, interphase exchange coupling improves with increasing annealing time, up to 2 min ( $H_c$  and  $M_r$  increase, Figure 6.1a and the irreversible peak in the derivative shifts to higher applied field values 6.1b), but another 30 s of annealing time produces the opposite effect. When we increase the temperature to  $750 \text{ }^\circ\text{C}$  (Figure 6.1d) we see the same trend, improvement up to 1.5 min and then a decrease. Comparing with the samples milled for 8 h, the results remain the same at  $700 \text{ }^\circ\text{C}$  (Figure 6.2d) with a noticeable decrease in the interphase exchange coupling at 2.5 min, but not in the case of the samples annealed at  $750 \text{ }^\circ\text{C}$  (Figure 6.2d) where things seem to slightly improve at 2 min of annealing time ( $M_r$  remains the same, while  $H_c$  increases slightly). This behaviour is also reflected in the energy product. Increasing annealing time from 1.5 to 2 min at  $700 \text{ }^\circ\text{C}$  yields an increase from  $34$  to  $42 \text{ KJ/m}^3$  and  $3.3$  to  $25 \text{ KJ/m}^3$  for the 6 h and 8 h MM samples respectively, while further increasing annealing time to 2 min results in a significant drop to  $23$  and  $17 \text{ KJ/m}^3$  for the same samples. Again looking now at the samples annealed at  $750 \text{ }^\circ\text{C}$  we see that increasing annealing time from 1 to 2 minutes greatly improves the energy product from  $11$  to  $50 \text{ KJ/m}^3$  and from  $2$  to  $31 \text{ KJ/m}^3$  for the 6 h and 8 h MM samples respectively, while a further increase results in a loss of  $(BH)_{max}$  for the 6 h MM samples and a slight increase to  $32 \text{ KJ/m}^3$  for the 8 h MM sample. The diverging trends seen for the annealing temperature of  $750 \text{ }^\circ\text{C}$  suggest, in this case, that interphase exchange coupling is improved by the additional 2 h of milling time. This leads us to conclude that at 6 h MM, using



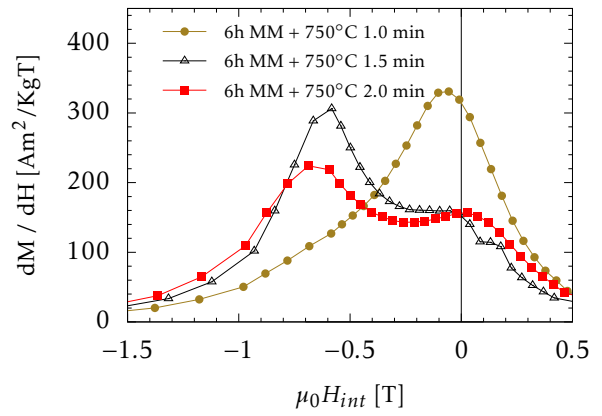
(a) Annealed at 700 °C for 1.5, 2 and 2.5 min



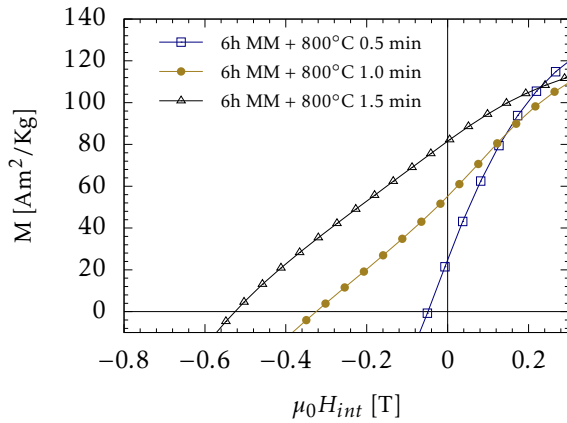
(b) Annealed at 700 °C for 1.5, 2 and 2.5 min



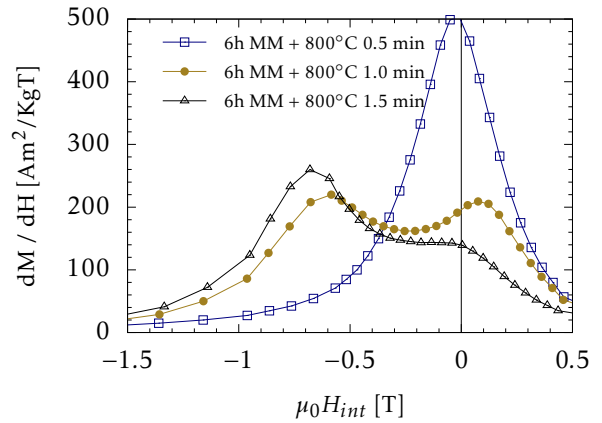
(c) Annealed at 750 °C for 1, 1.5 and 2 min



(d) Annealed at 750 °C for 1, 1.5 and 2 min

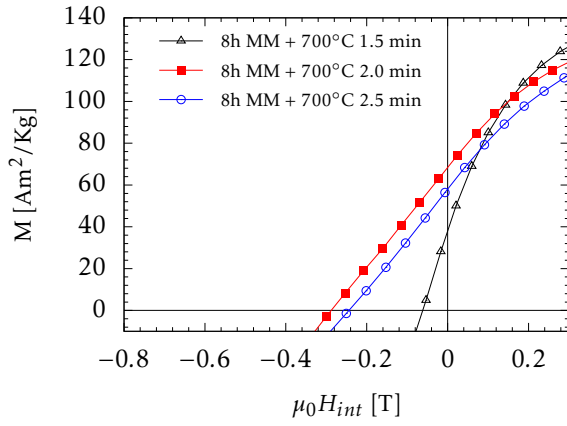


(e) Annealed at 800 °C for 0.5, 1 and 1.5 min

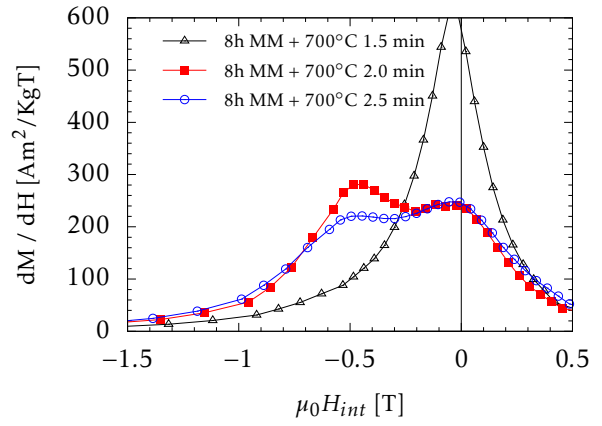


(f) Annealed at 800 °C for 0.5, 1 and 1.5 min

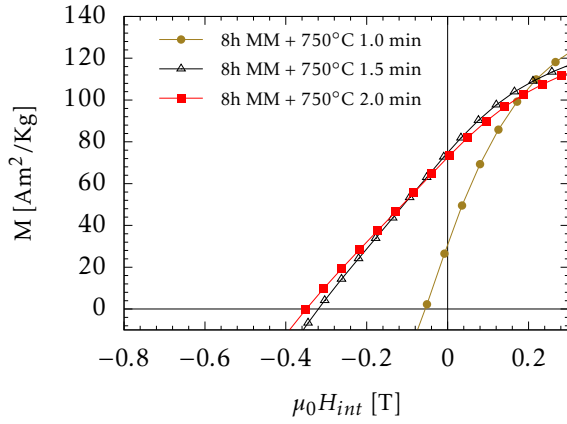
Figure 6.1: Demagnetization curves (a,c,e) and  $dM/dH$  vs  $H$  plots (b, d, f) for  $\text{Nd}_2\text{Fe}_{14}\text{B} + 10 \text{ wt\% MH-Fe}$  nanocomposites 6 h MM and annealed (as indicated)



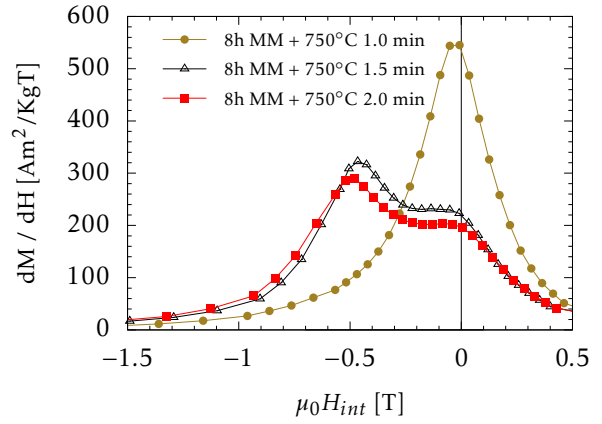
(a) Annealed at 700 °C for 1.5, 2 and 2.5 min



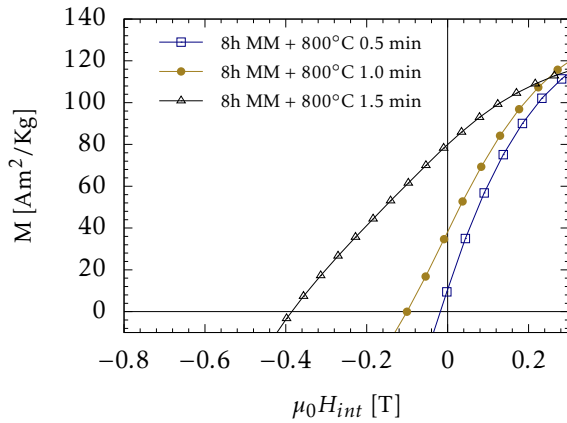
(b) Annealed at 700 °C for 1.5, 2 and 2.5 min



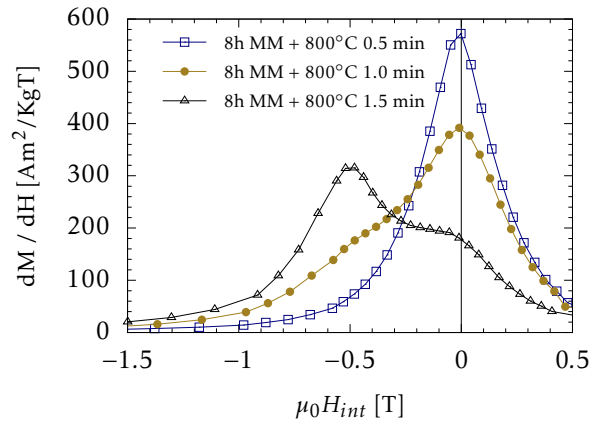
(c) Annealed at 750 °C for 1, 1.5 and 2 min



(d) Annealed at 750 °C for 1, 1.5 and 2 min



(e) Annealed at 800 °C for 0.5, 1 and 1.5 min



(f) Annealed at 800 °C for 0.5, 1 and 1.5 min

Figure 6.2: Demagnetization curves (a,c,e) and  $dM/dH$  vs  $H$  plots (b, d, f) for  $\text{Nd}_2\text{Fe}_{14}\text{B} + 10 \text{ wt}\% \text{ MH-Fe}$  nanocomposites 8 h MM and annealed (as indicated)

MH-Fe, even though average crystallite sizes are low 5 - 20 nm and comparable with those obtained for the samples using unhardened  $\alpha$ -Fe, the soft magnetic phase particles<sup>1</sup> become too large to be effectively pinned by the  $\text{Nd}_2\text{Fe}_{14}\text{B}$  phase. Moreover if this behaviour was to be driven by defects, we would expect that the samples milled for a longer duration would present an even lower degree of interphase exchange coupling as their defect density is much higher than that of the samples milled for only 6 h (as was concluded in Section 5). The samples annealed at 800 °C show only an improvement in magnetic properties, for the annealing times studied (up to 1.5 min).

---

<sup>1</sup>crystallite sizes are expected to be small, especially in the case of the hardened Fe which was milled for 4 additional hours, and was not annealed before being used in the starting powder. Moreover average crystallite sizes give us a good idea of particle growth rates, but do not necessarily inform on their size or shape

## 6.2 Effect of Phase Dispersal in Starting Powder Mixture on the Interphase Exchange Coupling in Hard-Soft Magnetic Nanocomposites

### 6.2.1 Synthesis

The  $\text{Nd}_2\text{Fe}_{14}\text{B} + 10\text{wt}\%$  Fe nanocomposite samples were created in the manner described in Section 4.4.1. Additionally three powder mixtures were created by varying the type of Fe powder, and mixing method (Table 6.1).

Table 6.1: Powder characteristics and premixing method for each of the three  $\text{Nd}_2\text{Fe}_{14}\text{B}+10\text{wt}\%$ Fe starting powders

Sample ID	$\text{Nd}_2\text{Fe}_{14}\text{B}$ powder 90wt%	Fe powder 10wt%	Mixing Method
S1	Particle size < 500 $\mu\text{m}$	Particle size < 100 $\mu\text{m}$	By hand
S2	Particle size < 500 $\mu\text{m}$	Particle size < 1 $\mu\text{m}$	By hand
S3	Particle size < 500 $\mu\text{m}$	Particle size < 1 $\mu\text{m}$	Turbula mixer

### 6.2.2 Structure and Microstructure Studies

XRD patterns for all milled and annealed samples show an increase in the crystallinity of both the  $\text{Nd}_2\text{Fe}_{14}\text{B}$  and  $\alpha\text{-Fe}$  phases as the annealing temperature increases from 700 to 800  $^\circ\text{C}$ . No significant differences could be observed between the samples annealed at the same time and temperature. The average crystallite sizes, derived from XRD measurements, for the soft magnetic phase present the same behavior for all three starting powder types, the Fe < 1  $\mu\text{m}$  starting powder yielding the same values (within the experimental error) as the Fe < 100  $\mu\text{m}$  starting powder.

### 6.2.3 Magnetic Properties of $\text{Nd}_2\text{Fe}_{14}\text{B} + 10 \text{ wt}\%$ Fe nanocomposites

The magnetic properties of the 6 h MM and annealed nanocomposite samples were studied using demagnetization curve. In the case of the samples made using Fe<100 $\mu\text{m}$ , Figure 6.3a, increasing annealing temperature from 700 to 800  $^\circ\text{C}$  improves the coercivity of the samples from 0.55 to 0.64 T, a 16% improvement. However remanence decreases from 113  $\text{Am}^2/\text{Kg}$  at 700  $^\circ\text{C}$  to 109  $\text{Am}^2/\text{Kg}$  after annealing at 800  $^\circ\text{C}$ , a 3% decrease. Of course, this translates into an overall gain, as the energy product slightly increases for 107 to 110  $\text{KJ}/\text{m}^3$ . Moving on to the the Fe<1  $\mu\text{m}$  - HM samples we see a similar behavior, Figure 6.3c, as  $H_c$  increases from 0.58 to 0.68 T, a 17% increase while  $M_r$  also increases in this case from 98 to 108  $\text{Am}^2/\text{Kg}$  leading to an energy product of 118  $\text{KJ}/\text{m}^3$ . The last sample set, the one mixed using the Turbula mixer, Figure 6.3e, even though it presents the lowest  $H_c$  values, 0.51 T at 700  $^\circ\text{C}$  and 0.62 T at 800  $^\circ\text{C}$  it presents

the highest remanence values of all the sets, with an  $M_r$  of  $115 \text{ Am}^2/\text{Kg}$  after annealing at  $700 \text{ }^\circ\text{C}$  which increases to  $117 \text{ Am}^2/\text{Kg}$  after annealing at  $800 \text{ }^\circ\text{C}$ ; this leads to the largest energy product of all the samples  $123 \text{ KJ}/\text{m}^3$ .

The quality of the magnetic interphase exchange coupling was further evaluated by  $dM/dH$  vs  $H$  plots (see Section 4.3.2), the data is shown in Figures 6.3b, 6.3d and 6.3f. The samples annealed for 1.5 min at  $700 \text{ }^\circ\text{C}$  (Figure 6.3b) present a similar behaviour, with a large peak at high field (around 0.6 T) and a very small one at low values of  $H$ . As the annealing temperature is increased to  $750 \text{ }^\circ\text{C}$  (Figure 6.3d) the samples produced with  $\text{Fe} < 1 \text{ } \mu\text{m}$  show a much higher peak at high fields than the sample produces with the starting powder containing larger Fe particles ( $< 100 \text{ } \mu\text{m}$ ). All other things being the same it is possible that the smaller grains allow for a better dispersal of the Fe particles which in turn leads to improved magnetic interphase exchange coupling. At the highest annealing temperature (Figure 6.3f) the samples produced with  $\text{Fe} < 1 \text{ } \mu\text{m}$  still present the higher peaks at high field. The samples which were mixed by hand show a very small peak at low field while the ones mixed with a Turbula mixer do not. Continuing our previous reasoning (where we discussed the enhanced  $M_r$  and  $(BH)_{max}$ ) we could conclude that the slight improvement in exchange coupling is due to the the improved dispersal of  $\alpha\text{-Fe}$  in the  $\text{Nd}_2\text{Fe}_{14}\text{B}$  starting powder by using the Turbula Mixer.

The energy product  $(BH)_{max}$  was calculated for the 6 h MM and annealed samples. The samples prepared with  $\text{Fe} < 1 \text{ } \mu\text{m}$  show an increase in the energy product with the increase in annealing temperature, while for the samples prepared with the powder mixture containing larger Fe particles the energy product remains relatively constant. The highest energy value  $123 \text{ kJ}/\text{m}^3$  was recorded for the samples prepared using the Turbula Mixer, a value at least 5% higher than that of the  $\text{Fe} < 100 \text{ } \mu\text{m}$  - HM and  $\text{Fe} < 1 \text{ } \mu\text{m}$  - HM annealed in the same manner. Therefore it seems that increasing the homogeneity of the starting powder, by mechanically mixing the initial phases, slightly improves the performance of the nanocomposite samples.

### 6.3 Partial Conclusions

In summary, we have shown that for the suitable formation of exchange coupled hard-soft nanocomposites through mechanical milling, the difference in mechanical hardness between the two constituent phases plays a very significant role and should be kept as low as possible. Hardness disparity delays the beginning of the composite formation process and increases the requirements for both crack formation and particle welding. All this leads to a less optimal microstructure and a high defect density i.e. large particle sizes for the soft magnetic phase and a lower anisotropy in the case of the hard magnetic phase.

To conclude, increasing the homogeneity of the starting powder slightly increases magnetic performance in  $\text{Nd}_2\text{Fe}_{14}\text{B} + 10\% \alpha\text{-Fe}$  obtained by mechanical milling. This is reflected in increased

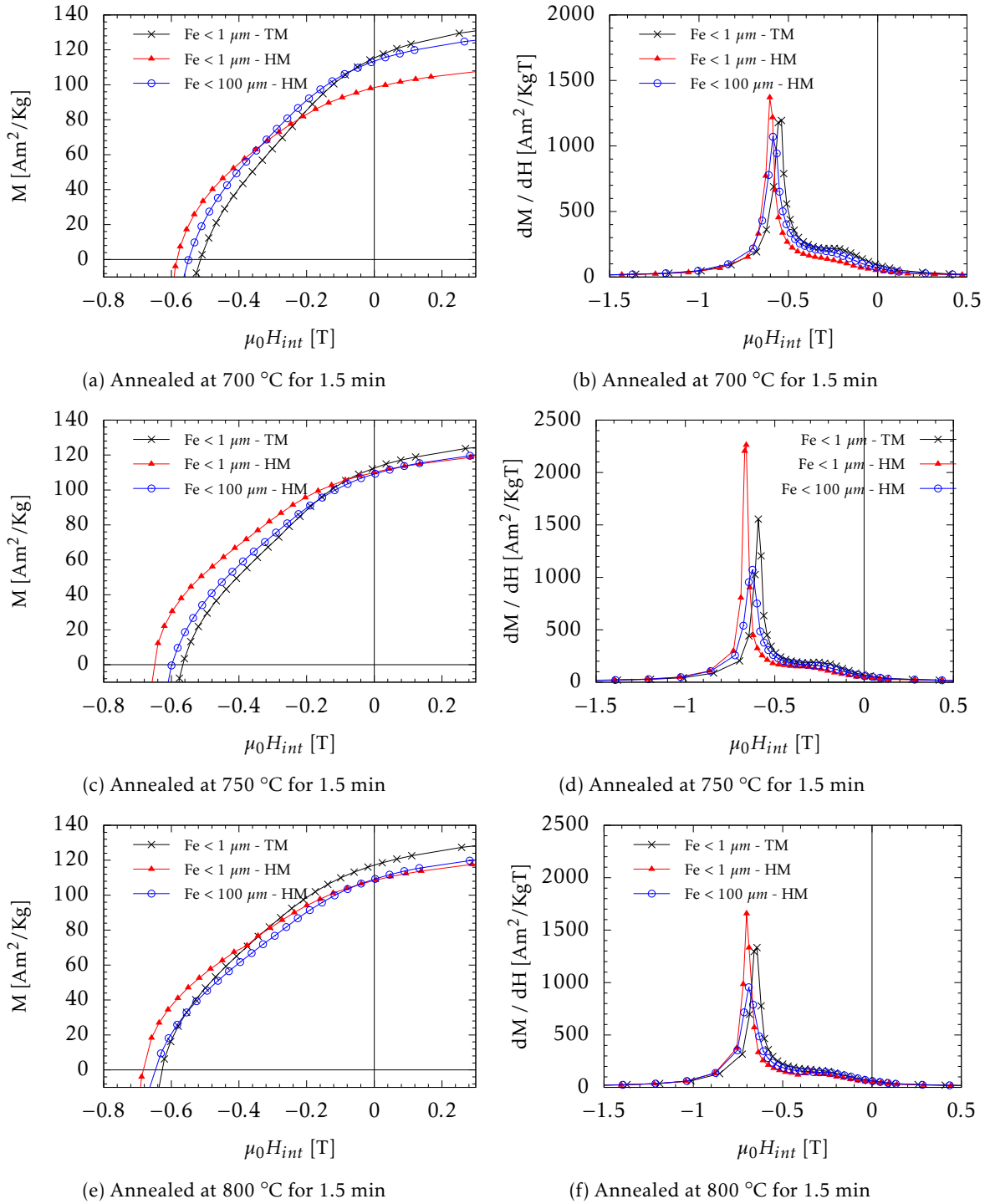


Figure 6.3: Demagnetization curves (a, c, e) and  $dM/dH$  vs  $H$  plots (b, d, f) for  $\text{Nd}_2\text{Fe}_{14}\text{B}$  + 10 wt% Fe 6 h MM and annealed (as indicated) nanocomposites

$M_r$  (5-10% in comparison to the other sample sets) and  $(BH)_{max}$  values. The highest energy product of  $123 \text{ kJ/m}^3$  being obtained for the sample premixed using a Turbula Mixer.

## Chapter 7

# Effect of Milling Energy on the Microstructure and Hard-Soft Exchange Coupling in Nanocomposite Magnetic Materials Obtained Trough Mechanical Milling

### 7.1 Synthesis

The  $\text{Nd}_2\text{Fe}_{14}\text{B} + 10\text{wt}\%$  Fe nanocomposite samples were created in the manner described in Section 4.4.1. The values for the milling energy were obtained trough computer simulations in the manner described by Abdellaoui and Gaffet.

Table 7.1: Milling media used for each data set

	Number of Balls	Ball Diameter $\varnothing$ (mm)
1	209	5
2	26	10
3	9	15
4	4	20

## 7.2 Structure and Microstructure Studies

As we shown before, during the milling process, the crystal structure of both phases is severely damaged. In order to improve the crystallinity of the hard magnetic phase, while also keeping the crystallite sizes of  $\alpha$ -Fe as small as possible, the as-milled powders were annealed for 1.5 min at 700, 750 and 800 °C. We can see that the  $\text{Nd}_2\text{Fe}_{14}\text{B}$  peaks become well resolved for all samples as temperature increases, therefore we can conclude that the crystallinity of all the samples improves with the increase in temperature. The samples milled with  $\varnothing = 20$  mm diameter balls present the highest degree of amorphisation (clearly visible for annealing at 700 °C, where the thermal energy supplied by the furnace is lower), followed by the samples milled with  $\varnothing = 5$  mm diameter balls, while the other samples present the highest degree of crystallinity with no significant differences between each other. This behaviour can be explained when taking into account the fact that the fracture initiation and fracture growth energy increases as the particle sizes decrease [71, 72]. This means that the effectiveness of the fracturing and re-welding process involved in milling becomes less efficient (especially for smaller impact energy) as the powder particles decrease in size during the milling process. As by increasing the impact energy, the fracturing process becomes more efficient, leading to the high degree of amorphisation seen in the samples milled with 20 mm diameter balls, as they have the largest energy per impact. On the other hand, the amorphisation seen in the samples milled with the 5 mm diameter balls can be explained by the high impact rate, and high total energy. This milling regime should produce a very large number of defects, even if the fracturing and re-welding process is less efficient.

The evolution of the structure and microstructure for the milled and  $\text{Nd}_2\text{Fe}_{14}\text{B} + 10$  wt% Fe samples was evaluated trough XRD and SEM. The investigation of the microstructure trough XRD revealed that the average crystallite sizes of the soft magnetic phase are largely independent of the milling energy. For the milling energies investigated the size of the Fe grains varies only with annealing temperature. This is most likely due to the ductile nature of Fe. On the other hand, the values of the average crystallite sizes, for the brittle  $\text{Nd}_2\text{Fe}_{14}\text{B}$  phase decrease (down to approximately 25 nm) as the impact energy increases due to the increased efficiency of the fracturing and re-welding process for small particles during mechanical milling.

## 7.3 Magnetic Properties of $\text{Nd}_2\text{Fe}_{14}\text{B} + 10$ wt%Fe nanocomposites obtained by different milling energy.

The magnetic proprieties of the 6 h MM and annealed  $\text{Nd}_2\text{Fe}_{14}\text{B} + 10$  wt% Fe samples were investigated trough demagnetization curves. These measurements show that the magnetic properties of all the samples improve with increasing annealing temperature, as both  $H_c$  and  $M_r$  increases due to the diminution of the defect density in the hard magnetic phase, which leads to an increase

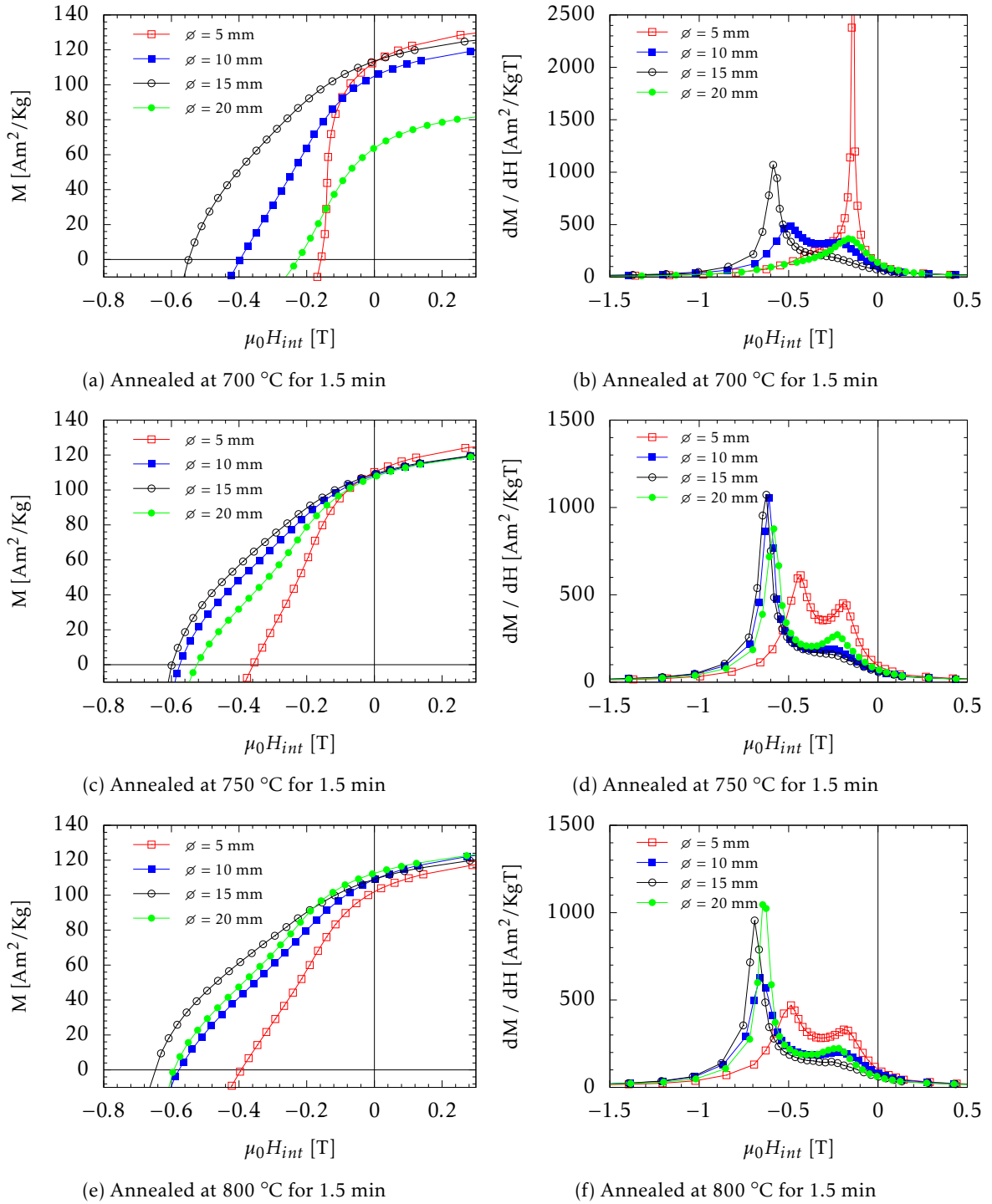


Figure 7.1: Demagnetization curves (a, c, e) and  $dM/dH$  vs  $H$  plots (b, d, f) for  $\text{Nd}_2\text{Fe}_{14}\text{B} + 10 \text{ wt}\%$  6 h MM and annealed (as indicated) nanocomposites

in its anisotropy, thus allowing for the better pinning of the soft magnetic inclusions. We see that the lowest coercivity, at all annealing temperatures, belongs to the samples milled using the 5 mm  $\varnothing$  balls. This is a result of the fact that the milling energy per impact is low (6 mJ/impact) and hence the crystalite sizes of the hard phase are the largest, 40-50 nm, where the optimum would be around 20 nm [29, 30], moreover due to the high impact frequency they also present a very large number of defects, in comparison with the other samples. The weak interphase magnetic coupling in these samples is especially obvious in the  $dM/dH$  vs  $H$  plots Figure 7.1 (b,d,f), where they consistently present two peaks, with a large intensity for the peaks at low field (around 0.1-0.2), a strong indication of ineffective interphase exchange coupling. However when the impact energy is increased to 34 mJ/impact, the average grain sizes for  $\text{Nd}_2\text{Fe}_{14}\text{B}$  decrease, resulting in a much higher value for  $H_c$  than that recorded for the samples milled with 5 mm  $\varnothing$  balls. Further increasing the impact energy, by using the 15 mm  $\varnothing$  balls further decreases the grain sizes of the hard magnetic phase and again leads to coercivity enhancement and improved smoothness of the demagnetization curve. This fact is also reflected in the  $dM/dH$  vs  $H$  plots, as at all annealing temperatures, for this sample set we mostly see a large peak at high field values, indicative of a good degree of exchange coupling. Increasing the milling energy to 124 mJ/impact ( $\varnothing = 20$  mm balls) does not lead to further reduction of grain sizes, however it severely decreases the magnetic properties of the composite samples. It is very likely that the increased stress and defect density is responsible for the observation, because increasing the annealing temperature hugely improves both remanence and coercivity. The the important increase in both  $H_c$  and  $M_r$  with annealing temperature (as more and more defects are removed) is evidence that the composite formation process was effective, but the magnetic properties of the sample are severely affected by defects and stress. Moreover the  $dM/dH$  vs  $H$  plots for the samples milled at 124 mJ/impact ( $\varnothing = 20$  mm balls) show only one small peak at low fields after annealing at 700 °C, due to the poor crystallinity of the hard magnetic phase. The single peak implies that the coercivity of the hard phase is comparable with the one of soft phase. Increasing annealing temperature causes the appearance of a very intense peak at high field values, which suggests that the anisotropy of the  $\text{Nd}_2\text{Fe}_{14}\text{B}$  phase is increased through the improvement of its crystallinity, however the smoothness of the demagnetization curve suggests that some soft phase inclusions remain unpinned by the hard magnetic phase.

The high coercivity and energy product (at all annealing temperatures) of the samples milled with 15 mm diameter balls are result of both the very small mean crystallite sizes of the hard and soft magnetic phases (ensuring good magnetic coupling), and the lower overall degree of amorphisation induced by the milling process. This leads us to the idea that for these samples a very good balance was struck between the impact energy and the total milling energy, yielding (after annealing) a favourable structure and microstructure for interphase exchange coupling.

## 7.4 Partial Conclusions

In summary,  $\text{Nd}_2\text{Fe}_{14}\text{B} + 10 \text{ wt\% Fe}$  nanocomposites were produced through mechanical milling at different energies induced by different milling balls (using  $\varnothing = 5, 10, 15$  and  $20$  mm diameter balls) and subsequent annealing at  $700, 750$  and  $800$  °C for  $1.5$  min. The average crystallite sizes of the hard magnetic phase mainly depend on the impact energy. In the investigated range of milling conditions, the higher the impact energy, the lower the mean crystallite sizes become (down to a limit of approximately  $25$  nm). The average crystallite sizes for  $\alpha\text{-Fe}$  phase of about  $10$  nm, are largely unaffected by the change in milling energy but increases significantly upon increasing the annealing temperature. The mean crystallite size (of both phases) influences the interphase exchange coupling, as the smaller crystallite sizes result in a better coupling between the hard  $\text{Nd}_2\text{Fe}_{14}\text{B}$  and soft  $\alpha\text{-Fe}$  phase. Increasing the milling energy also leads to an increase in the amorphisation of the crystalline structure of the hard magnetic phase which means that in order to restore the crystallinity, higher temperatures or longer annealing times are required which in turn leads to the significant growth of the  $\alpha\text{-Fe}$  crystallites. This reduces the effectiveness of the interphase exchange coupling and consequently optimized conditions have to be found. The best results for the studied nanocomposites were obtained for the samples milled with  $\varnothing = 15$  mm diameter steel balls and annealed at  $800$  °C:  $H_c = 0.65$  T,  $M_r = 108$  Am<sup>2</sup>/Kg and  $(BH)_{max} = 110$  KJ/m<sup>3</sup>.

## Chapter 8

# Effect of Spark Plasma Sintering on Hard-Soft Interphase Exchange Coupling in Magnetic Nanocomposite Powders

### 8.1 SPS Magnets Based on $\text{Nd}_2\text{Fe}_{14}\text{B} + 10\% \text{Fe}$ Nanocomposites

#### 8.1.1 Synthesis

$\text{Nd}_2\text{Fe}_{14}\text{B} + 10 \text{ wt}\% \alpha\text{-Fe}$  sintered nanocomposite samples were produced by ball milling (see Section 4.4.1) and subsequent spark plasma sintering. The starting powder (90 wt%  $\text{Nd}_2\text{Fe}_{14}\text{B} < 500 \mu\text{m}$  and 10 wt%  $\alpha\text{-Fe} < 1 \mu\text{m}$  mixed using a Turbula mixer) was milled for 6 h in a planetary ball mill. The resulting nanocomposite powder was then sintered in SPS installation. Sintering was done at a pressure of 35 MPa with a heating rate of 5 K/s and a cooling rate of 2K/s. The temperature was raised up to 700, 750 or 800 °C where it was kept stable for 2.5, 2 and 1.5 minutes respectively.

#### 8.1.2 Structural and Microstructural Studies

The structure and microstructure of the sintered nanocomposite samples was investigated using XRD. The diffraction patterns for the sintered samples show that the hard magnetic phase is well crystallized in after all applied sintering regimes, with only the peaks corresponding to the  $\text{Nd}_2\text{Fe}_{14}\text{B}$  and  $\alpha\text{-Fe}$  being visible. The average crystallite sizes were calculated for both the hard

and soft magnetic phases. The average crystallite sizes for Fe are very similar in all three cases, being situated around 22-23 nm, the upper acceptable limits for hard-soft interphase exchange coupling. The mean grain size for the  $\text{Nd}_2\text{Fe}_{14}\text{B}$  phase was also evaluated to be within the 31 to 33 nm range, which was previously found to be adequate for achieving a good degree of hard-soft exchange coupling.

The density of the sintered compacts was evaluated by measuring the volume and weight of the samples. The sample densities fall between 60 and 70 % of the theoretical value for the composite material. The densities were used later for the calculation of the polarization  $J$ .

### 8.1.3 Magnetic Properties of $\text{Nd}_2\text{Fe}_{14}\text{B} + 10 \text{ wt}\% \text{Fe}$ SPS nanocomposites

The magnetic behavior of the  $\text{Nd}_2\text{Fe}_{14}\text{B} + 10 \text{ wt}\% \alpha\text{-Fe}$  SPS compacts was studied through demagnetization curves and  $dM/dH$  vs  $H$  plots (Figure 8.1). The demagnetization curves, Figure 8.1a, show that the coercivity of the samples improves with increasing annealing temperature (as the hard phase is better recrystallized due to the increased temperature), but the smoothness of the curves is much worse than in the case of annealed powders (Figure 5.1). To elaborate, the concave shape of the curves indicates that our samples contain a significant amount of unpinned or poorly pinned  $\alpha$  Fe particles. This is not surprising as the average crystallite sizes for the soft magnetic phase are fairly large and thus most likely serve as nucleation sites for the investigated materials. The shape of the curve is better analyzed in the derivative (Figure 8.1b), where in all three cases we see two peaks, which signifies dual magnetic phase behavior instead of single, or almost single, which was evidenced in nanocomposite annealed powders, Figures 5.1 (b,d,f).

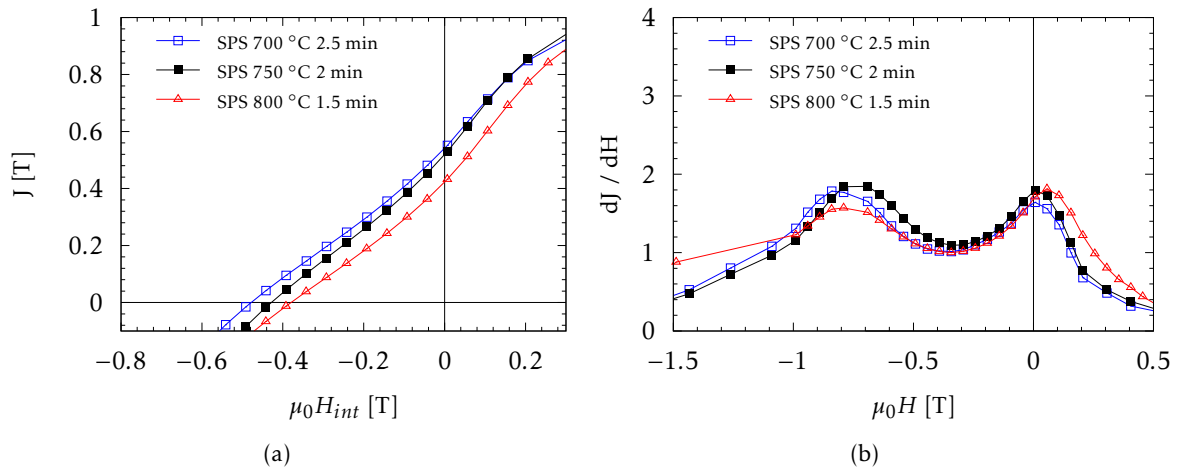


Figure 8.1: Demagnetization curves (a) and  $dM/dH$  vs  $H$  plots (b) for  $\text{Nd}_2\text{Fe}_{14}\text{B} + 10 \text{ wt}\% \text{Fe}$  SPS compacts sintered at 700, 750 and 800 °C.

The magnetic performance the  $\text{Nd}_2\text{Fe}_{14}\text{B} + 10\text{wt}\% \text{Fe}$  SPS samples is very poor, with energy

products ranging only between 6 and 15 KJ/m<sup>3</sup>, an order of magnitude lower than the results obtained for annealed powders.

## 8.2 SPS Magnets based on SmCo<sub>5</sub> + 20 wt% Fe Nanocomposites

### 8.2.1 Synthesis

The SPS compacts were produced by sintering SmCo<sub>5</sub> + 20 wt% Fe nanocomposite powder produced in the manner described in Section 4.4.2. The details of the SPS process were given in Section 4.1.3. The sintering time, temperature and pre-sintering annealing (if any) are summarized in table 8.1 for all samples. Pre-sintering annealing at 350 °C was performed in order to eliminate stress within the powder, in order to improve densification during the SPS process. As can be seen from Table 8.1 annealing leads to nearly doubling the density of the nanocomposite material (from 35 % density for sample P4 to 60 % for sample P6). The annealing at 600 °C was done in order to investigate the effect of sintering on a powder which already presented a good degree of interphase exchange coupling.

Table 8.1: Synthesis details and density for SmCo<sub>5</sub>+20wt%  $\alpha$ -Fe SPS compacts

Sample ID	Annealing	Sintering	Density	
			Kg/m <sup>3</sup>	% of Theoretical
Powder	600 °C 0.5 h	N/A	Theoretical	100
P4	N/A	600 °C 2 min	3013	35
P5	N/A	600 °C 6 min	4654	55
P6	350 °C 6 h	600 °C 2 min	5010	60
P7	600 °C 0.5 h	600 °C 2 min	5058	60
P8	600 °C 0.5 h	700 °C 2 min	5747	68

### 8.2.2 Structural and Microstructural Studies

The structure and microstructure of the sintered samples was investigated using XRD. Since some samples (P4 and P5) were measured using Cu K $\alpha$  radiation and others (P6, P7 and P8) were measured using Co K $\alpha$  radiation, the diffraction patterns were plotted over 1/d instead of 2 $\theta$ . We can see that the sintered samples contain both SmCo<sub>5</sub> and Sm<sub>2</sub>Co<sub>17</sub> as the hard magnetic phases, their coexistence is pointed out clearly by the two peaks at around 0.4 Å<sup>-1</sup>. Since we see no evidence of other phases and since the 1:5 phase does not form stable structures with iron we can say that most likely the formation of the 2:17 phase takes place by the infusion of iron from the soft magnetic phase, therefore the formula for the 2:17 structure would be of the form Sm<sub>2</sub>Co<sub>17-x</sub>Fe<sub>x</sub>. However from our measurements we can not estimate the value of x. Both phases seem to be

present at all SPS sintering temperatures, however the presence of  $\text{Sm}_2\text{Co}_{17}$  is most evident for the highest sintering temperature (P8) as the XRD peaks become sharper and the  $\text{Sm}_2\text{Co}_{17}$  (002) peak (situated on the right of strongest intensity reflection of this phase) emerges between the strongest reflections of both the  $\text{SmCo}_5$  phase and  $\alpha$  Fe.

Looking at the dependence of the average grain sizes of iron, before and after SPS, as a function of annealing temperature. For legibility reasons only the samples sintered at 600 °C were plotted. From this graph we can conclude that the increase in size is mostly due to the SPS sintering process as the difference in grain sizes before and after SPS is huge (nearly three times larger). Which can be extremely problematic as the minimum condition for pinning the soft phase inclusions is that their size can not exceed twice the magnetic domain wall length of the hard magnetic phase as discussed in section 3 (somewhere in the interval 5 nm for  $\text{SmCo}_5$  to 12 nm for  $\text{Sm}_2\text{Co}_{17}$ ).

### 8.3 Magnetic Properties of $\text{SmCo}_5 + 20 \text{ wt}\% \text{Fe}$ SPS Compacts

Demagnetization curves for  $\text{SmCo}_5 + 20 \text{ wt}\% \text{Fe}$  (Figure 8.2a) recorded at 300 K show that the sintered samples have comparable  $H_c$ . Excepting P4 the coercivity of all other samples falls within the 0.78-0.81 T interval. However the remanence is much lower for the SPS compacts compared to the un-sintered powder. Partially, this decrease can be attributed to the low density of the sintered samples (< 70% of theoretical value), but the shoulders seen in the demagnetization curves for the SPS compacts suggest that  $J_r$  is significantly affected by the inefficient pinning of the soft phase inclusions. From the  $dM/dH$  vs  $H$  plots (Figure 8.2b) we can see that the central peak positions of the sintered samples and the reference powder match (excluding P4 as the degree of interphase exchange coupling is quite poor in this case), the significant difference between the two being the broadness of the peaks. The very sharp peak profiles seen in the sintered samples can be attributed to the spread of magnetic domain reversal due to compaction. This effect is most visible in the reduction of energy product between the reference powder and sintered samples. Even if we consider that the SPS compacts have the theoretical density, P8 which has the highest  $(BH)_{max}$  of the compacts, only yields an energy product of 80  $\text{KJ/m}^3$  which means that the difference between it and the reference powder is due to the poor pinning of soft phase inclusions.

### 8.4 Partial Conclusions

The SPS method was successful at producing dense samples, however it is very likely that densification allows nucleation processes to propagate through the entire sample (as opposed to being confined to individual powder particles). This is assumed to significantly increase the proportion of seemingly low coercivity magnetic domains within the sintered samples. In the case of  $\text{Nd}_2\text{Fe}_{14}\text{B}$  SPS compacts it has been shown that the soft phase inclusions can be at least partially pinned. It

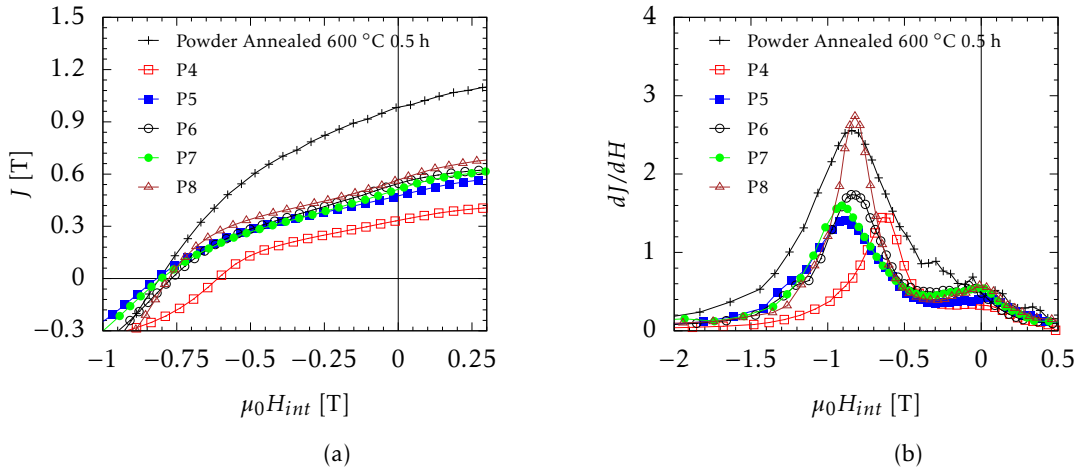


Figure 8.2: Demagnetization curves (a) and  $dM/dH$  vs  $H$  plots (b) for SmCo<sub>5</sub> + 20 wt% Fe SPS compacts

seems that even though XRD measurements show that the hard magnetic phase is fairly well crystallized and grain sizes for Fe are kept in check with reasonable success, improvements in both areas are required in order to achieve a good degree of hard-soft exchange coupling. Spark plasma sintering on SmCo<sub>5</sub> + 20% Fe magnetic nanocomposite powders has yielded much better results than in the case of Nd<sub>2</sub>Fe<sub>14</sub>B + 10% Fe SPS compacts. The ratio between well and poorly coupled magnetic domains, as analyzed through  $dM/dH$  vs  $H$  plots, is promising. The highest recorded values of  $H_c$  (0.81 T) from the demagnetization curves compare well with those measured on powder samples, while the values of  $J_r$  (0.59 T) could be feasibly increased by better control of the microstructure and density.

## Chapter 9

# Conclusions and Future Prospects

In this work we have set out to study the influence of the microstructure on the interphase exchange coupling in hard-soft magnetic nanocomposites and its influence on the magnetic properties of the material. Specifically we strove to alter the microstructure of the material by tweaking the synthesis process at its various stages. These modifications resulted in the creation of various nanocomposite microstructures, which could then be investigated so that their relationship with the magnetic properties of the spring magnets could be studied.

Our studies revolved around two nanocomposite materials:  $\text{Nd}_2\text{Fe}_{14}\text{B} + 10\text{wt}\% \alpha\text{-Fe}$  and  $\text{SmCo}_5 + 20\text{wt}\% \alpha\text{-Fe}$ . The hard magnetic phase was obtained by melting, annealing and finally grinding. The resulting powder was then milled alongside the soft magnetic phase. The composite powders were annealed and/or sintered. Therefore conceptually the synthesis process, itself, can be broken up into three main stages:

- The creation of the starting powder mixture
- Milling of the initial mixture
- Annealing and/or sintering the milled powders

where modifications at each stage produce different microstructures with different magnetic properties.

### **The Starting Powder Mixture Stage**

Because in hard-soft exchange coupled nanocomposites there exists a very intimate relationship between the magnetic properties and the size of the soft magnetic inclusions, at this stage we have attempted to limit their size, while not increasing milling time.

Premilling the soft magnetic phase lead to a significant increase in its mechanical hardness. This in turn resulted in a delay in the composite formation process while simultaneously increasing the amount of stress and the number of defects in the composite material. These aspects are reflected in a severe drop of the magnetic performance of the spring magnets. In contrast, improving the dispersion of the two phases which make up the starting mixture has proven effective, as the increased homogeneity of the starting powder resulted in enhanced energy products.

### **The Mechanical Milling Stage**

The effect of the milling energy on the microstructure, i.e. the interphase exchange coupling, of the  $\text{Nd}_2\text{Fe}_{14}\text{B} + 10\text{wt}\% \alpha\text{-Fe}$  nanocomposites was studied. The milling energy and impact frequency were tuned using different diameter balls. The energy per impact and the total energy were both evaluated by computer simulation. Our studies showed that the hard magnetic phase crystallite sizes decrease as the energy per impact increases due to additional fracture and re-welding events during the milling process. However, once a base value is reached, further increasing the impact energy only serves to further damage of the crystalline structure.

Magnetic studies have shown that by tuning the  $\text{Nd}_2\text{Fe}_{14}\text{B}$  crystallite sizes the energy product of the nanocomposites can be improved. This has been attributed to the fact that the nucleation field of the hard magnetic phase increases with decreasing crystallite sizes.

### **The Annealing and SPS Stage**

The main objective of the annealing followed the recovery of the anisotropy of the hard magnetic phase, by improving its crystallinity, destroyed by milling. Simultaneously, we took into account that the heat treatments should avoid, as much as possible, the growth of the soft phase crystallites. Considering the above objectives we used two types of annealing: classical annealing and short time annealing. Most of the studies were done using the short time annealing process, because our investigations proved that this type of heat treatment is better suited for obtaining the desired microstructures for hard-soft nanocomposites. Additionally, in order to improve the physical and magnetic properties of SPS compacts, pre-sintering annealing was also employed.

These result encouraged us to use SPS procedure to create both  $\text{Nd}_2\text{Fe}_{14}\text{B} + 10\text{wt}\%\text{Fe}$  and  $\text{SmCo}_5 + 20\text{wt}\%\text{Fe}$  compacts. It was shown that compaction favors the propagation of magnetic domain reversal throughout the entire sample, diminishing the energy products previously attained in annealed powders. It should also be noted that  $\text{SmCo}_5/\text{Fe}$  compacts achieved energy products over four times greater than  $\text{Nd}_2\text{Fe}_{14}\text{B}/\text{Fe}$  compacts. This observation could be attributed to the fact that the  $\text{SmCo}_5$  hard magnetic phase is inherently a much more anisotropic material. However, given the limited data sets currently available the assertion regarding the difference in magnetic performance should be taken as speculation. Moreover additional data could shed some extra light into the matter and will make the subject of future study. Furthermore the improvement of  $(BH)_{max}$

in SPS compacts, due to modest densities, could be achieved by increasing the compact densities and optimizing the composite nanostructure.

# Publications

## On Thesis Subject

- S. Mican, **R. Hirian**, O. Isnard, I. Chicina, V. Pop, "Effect of Milling Conditions on the Microstructure and Interphase Exchange Coupling of  $\text{Nd}_2\text{Fe}_{14}\text{B}/\alpha\text{-Fe}$  Nanocomposites", *Physics Procedia* 75 (2015) 1314-1323
- **R. Hirian**, S. Mican, B. Neamțu, V. Pop, "Surfactant Effect on the Structural and Magnetic Properties of Fe Powders Prepared by Wet Milling", *Studia UBB Physica* 60 (2015) 53-58
- S. Mican, **R. Hirian**, L. V. B. Diop, I. Chicinaș, O. Isnard, V. Pop, —Microstructure and Interphase Coupling in  $\text{Nd}_2\text{Fe}_{14}\text{B}/\alpha\text{-Fe}$  Nanocomposites Obtained By Mechanical Milling and Short Time Annealing", *Romanian Journal of Physics* 61 (2016) 506-517
- **R. Hirian**, **S. Mican**, O. Isnard, L. Barbu-Tudoran and V. Pop, "Effect of Starting Powder Premixing on the Interphase Exchange Coupling in  $\text{Nd}_2\text{Fe}_{14}\text{B} + 10 \text{ wt} \% \text{ Fe}$  Nanocomposites Obtained Through Mechanical Milling", *Studia UBB Physica* 61 (2016) 55-64
- **R. Hirian**, S. Mican, O. Isnard, L. Barbu-Tudoran, V. Pop, "Influence of microstructure on the interphase exchange coupling of  $\text{Nd}_2\text{Fe}_{14}\text{B} + 10 \text{ wt} \% \alpha\text{-Fe}$  nanocomposites obtained at different milling energies", *Journal of Alloys and Compounds* 697 (2017) 19-24
- **R. Hirian**, A. Bolinger, O. Isnard and V. Pop, "Influence of High Anisotropy Phase on the Properties of Hard-Soft Magnetic Nanocomposite Powders Obtained by Mechanical Milling" submitted to *Powder Metallurgy*
- **R. Hirian**, B. V. Neamțu, A. Ferenczi, O. Isnard, I. Chicinaș and V. Pop, "Exchanged Coupled  $\text{SmCo} /\alpha\text{-Fe}$  Nanocomposite Magnets Obtained by Mechanical Milling and Spark Plasma Sintering" to be submitted

## Other Work During PHD Period

- S. Mican, D. Benea, **R. Hirian**, R. Gavrea, O. Isnard, V. Pop, M. Coldea, "Structural, electronic and magnetic properties of the  $\text{Mn}_{50}\text{Al}_{46}\text{Ni}_4$  alloy", *Journal of Magnetism and Magnetic Materials* 401 (2016) 841-847
- R. Gavrea, **R. Hirian**, S. Mican, D. Benea, O. Isnard, M. Coldea, V. Pop, Structural, electronic and magnetic properties of the  $\text{Mn}_{54-x}\text{Al}_{46}\text{Ti}_x$  ( $x = 2; 4$ ) alloys, *Intermetallics* 82 (2017) 101-106

# Presentations and Summer Schools

## Presentations - On Thesis Subject

- Poster - S. Mican, R. Hirian, O. Isnard, I. Chicinaş and V. Pop, "Effect of Milling Conditions on the Microstructure and Interphase Exchange Coupling of  $Nd_2Fe_{14}B/\alpha$ -Fe Nanocomposites", **International Conference on Magnetism ICM2015**, 5-10 July 2015, Barcelona, Spain
- Poster - R. Hirian, S. Mican, L. V. B. Diop, I. Chicinaş, O. Isnard and V. Pop, "Influence of Milling Conditions on the Hard/Soft Exchange Coupling of the Short Time Annealed  $Nd_2Fe_{14}B/\alpha$ -Fe Nanocomposite", **International Summer School Physical and Chemical Principles in Materials Science**, 6-17 July 2015, Xi'An, China
- Poster - S. Mican, R. Hirian, O. Isnard, I. Chicinaş and V. Pop, "Effect of Milling Energy on the Interphase Exchange Coupling of  $Nd_2Fe_{14}B/\alpha$ -Fe Nanocomposites", **European Summer School on Magnetism**, 24 August - 4 September 2015, Cluj-Napoca, Romania
- Oral - R. Hirian, S. Mican, O. Isnard, L. Barbu-Tudoran and V. Pop, "Effect of Starting Powder Premixing on the Interphase Exchange Coupling in  $Nd_2Fe_{14}B + 10wt\%$  Fe Nanocomposites Obtained Through Mechanical Milling", **16<sup>th</sup> International Balkan Workshop on Applied Physics and Materials Science**, 7-9 July 2016, Constanţa, Romania
- Poster - R. Hirian, S. Mican, O. Isnard and V. Pop, "The Influence of Short Time Heat Treatment on the Microstructure and Magnetic Behavior of the  $SmCo_5/\alpha$ -Fe Nanocomposite Obtained by Mechanical Milling", **Joint European Magnetism Symposia JEMS2016**, 21-26 August 2016, Glasgow Scotland
- Poster - R. Hirian, S. Mican, O. Isnard, L. Barbu-Tudoran and V. Pop, "Influence of Microstructure on the Interphase Exchange Coupling of  $Nd_2Fe_{14}B + 10 wt\%$  Fe Nanocomposites Obtained by Mechanical Milling", **Rare Earth Permanent Magnets REPM2016** 28 August - 1 September, Darmstadt, Germany
- Oral - R. Hirian, S. Mican, O. Isnard, L. Barbu-Tudoran and V. Pop, "Influence of Microstructure on the Interphase Exchange Coupling of  $Nd_2Fe_{14}B + 10wt\%$   $\alpha$ -Fe Nanocomposites Obtained at

*Different Milling Energies*", **2nd Poznań School of Physics of NanoMagnetism POSNAMAG 2017** 21-30 June 2017 Poznań, Poland

- Poster - **R. Hirian**, R. Gavrea, B. V. Neamțu, A. Ferenczi, O. Isnard, I. Chicinaș, V. Pop, "Exchanged Coupled  $\text{SmCo}_5/\alpha\text{-Fe}$  Nanocomposite Magnets Obtained by Mechanical Milling and Spark Plasma Sintering", **INTERMAG 2017** 24-28 April. 2017, Dublin, Ireland
- Oral - **R. Hirian**, A. Bolinger, O. Isnard and V. Pop, "The influence of hard phase on the magnetic behavior of hard/soft exchange coupled nanocomposite powders obtained by mechanical milling", **RoPM & AM 17** 17 - 20 September 2017, Cluj-Napoca, Romania

## Presentations - Other Work During PHD Period

- Poster - **R. Hirian**, S. Mican, O. Isnard, I. Chicinaș, M. Coldea and V. Pop, "Structural and Magnetic Properties of Mechanically Milled  $\text{Mn}_{50}\text{Al}_{46}\text{T}_4$  ( $T = \text{Mn}, \text{Ni}$ ) Alloys", **International Conference on Magnetism ICM2015**, 5-10 July 2015, Barcelona, Spain
- Poster - R. Gavrea, **R. Hirian**, S. Mican, D. Benea, O. Isnard, M. Coldea and V. Pop, "Structural and electronic and magnetic properties of  $\text{Mn}_{54-x}\text{Al}_{46}\text{Ti}_x$  ( $x = 2 ; 4$ ) alloys", **Rare Earth Permanent Magnets REPM2016** 28 August - 1 September, Darmstadt, Germany
- Poster - G. Souca, R. Dudric, S. Mican, **R. Hirian**, R. Tetean "Magnetic Properties and Magnetocaloric Effect on  $\text{Ce}_{1-x}\text{Y}_x\text{Fe}_2$ ", **International Summer School Physical and Chemical Principles in Materials Science**, 7-16 July 2016 Paris, France
- Poster - **R. Hirian**, T.-L. Biter, A. Boiciuc, O. Isnard and V. Pop, "Structural and magnetic behavior of the LTP  $\text{MnBi}$  phase", **The European Conference PHYSICS OF MAGNETISM 2017 PM'17** June 26-30, 2017 Poznań, Poland

## Summer Schools Attended

- International Summer School Physical and Chemical Principles in Materials Science, 6-17 July 2015, Xi'An, China
- European Summer School on Magnetism, 24 August - 4 September 2015, Cluj-Napoca, Romania
- 2nd Poznań School of Physics of NanoMagnetism POSNAMAG 2017, 21-30 June 2017 Poznań, Poland

# Bibliography

- [1] R. Skomski, P. Manchanda, P. K. Kumar, B. Balamurugan, A. Kashyap, and D. J. Sellmyer. Predicting the future of permanent-magnet materials. *IEEE Transactions on Magnetics*, 49(7):3215–3220, 2013.
- [2] J. M. D. Coey. Permanent magnets: Plugging the gap. *Scripta Materialia*, 67(6):524–529, 2012.
- [3] A. Zhukov. *Novel Functional Magnetic Materials*. Springer, series in edition, 2016.
- [4] Workshop on "Energy and Materials Criticality, Santorini". <http://www.physics.udel.edu/emc/index.html>, aug 2013.
- [5] Trilateral EU-Japan-U.S. Conference on Critical Materials for a Clean Energy Future, Washington DC, ". oct 2011.
- [6] J. S. Jiang. Magnetization processes in core/shell exchange-spring structures. *Journal of Applied Physics*, 117(17):17A734, 2015.
- [7] Narayan Poudyal and J Ping Liu. Advances in nanostructured permanent magnets research. *Journal of Physics D: Applied Physics*, 46(4):043001, 2013.
- [8] D. J. Sellmyer, B. Balamurugan, B. Das, P. Mukherjee, R. Skomski, and G. C. Hadjipanayis. Novel structures and physics of nanomagnets (invited). *Journal of Applied Physics*, 117(17):172609, 2015.
- [9] Rajasekhar Madugundo and George C. Hadjipanayis. Anisotropic mn-al-(c) hot-deformed bulk magnets. *Journal of Applied Physics*, 119(1):013904, 2016.
- [10] P. Tozman, M. Venkatesan, and J. M. D. Coey. Optimization of the magnetic properties of nanostructured y-co-fe alloys for permanent magnets. *AIP Advances*, 6(5):056016, 2016.
- [11] Imants Dirba, Philipp Komissinskiy, Oliver Gutfleisch, and Lambert Alff. Increased magnetic moment induced by lattice expansion from -fe to -fe8n. *Journal of Applied Physics*, 117(17):173911, 2015.

- [12] Semih Ener, Johannes Kroder, Konstantin P. Skokov, and Oliver Gutfleisch. The search for room temperature tetragonal phases of fe-mn-ga: A reactive crucible melting approach. *Journal of Alloys and Compounds*, 683(Supplement C):198 – 204, 2016.
- [13] David J. Sellmyer. Applied physics: Strong magnets by self-assembly. *Nature*, 420:374 – 375, 2002.
- [14] R. Skomski. Aligned twophase magnets: Permanent magnetism of the future? (invited). *Journal of Applied Physics*, 76(10):7059–7064, 1994.
- [15] E. F. Kneller and R. Hawig. The exchange-spring magnet: A new material principle for permanent magnets. *IEEE Transactions on Magnetics*, 27(4):3588–3600, 1991.
- [16] V. Pop, S. Gutoiu, E. Dorolti, O. Isnard, and I. Chicina. The influence of short time heat treatment on the structural and magnetic behaviour of Nd<sub>2</sub>Fe<sub>14</sub>B/ $\alpha$ -Fe nanocomposite obtained by mechanical milling. *Journal of Alloys and Compounds*, 509:9964–9969, 2011.
- [17]
- [18] Rodrigue Lardé, Jean-Marie Le Breton, Adeline Matre, Denis Ledue, Olivier Isnard, Viorel Pop, and Ionel Chicina. Atomic-scale investigation of smco5/-fe nanocomposites: Influence of fe/co interdiffusion on the magnetic properties. *The Journal of Physical Chemistry C*, 117(15):7801–7810, 2013.
- [19] Etienne du Tremolet de Lacheisserie. *Magnetism Fundamentals*. Springer Science, 2005.
- [20] J. M. D. Coey. *Magnetism and Magnetic Materials*. Cambridge University Press, 2009.
- [21] R. Skomski and J. M. D. Coey. Magnetic anisotropy How much is enough for a permanent magnet ? *Scripta Materialia*, 112:3–8, 2016.
- [22] P. K. Sahota, Y. Liu, R. Skomski, P. Manchanda, and R. Zhang. Ultrahard magnetic nanostructures. *Journal Of Applied Physics*, 345(111), 2012.
- [23] J. Jiang and Y. Wang. Effect of the first hot extrusion temperature on microstructure and magnetic properties of second-extrusion Nd<sub>2</sub>Fe<sub>14</sub>B /  $\alpha$ -Fe nanocomposite. *Journal of Magnetism and Magnetic Materials*, 332:76–80, 2013.
- [24] X. Jiang. *Structural, magnetic and microstructural studies of composition-modified Sm-Co ribbons*. PhD thesis, University of Nebraska, 2014.
- [25] H. Su Ryo, L. X. Hu, and Y. L. Yang. Micromagnetic study for magnetic properties of exchange coupled nanocomposite magnetic systems with Nd<sub>2</sub>Fe<sub>14</sub>B grains embedded in  $\alpha$ -Fe matrix. *Journal of Magnetism and Magnetic Materials*, 426:46–52, 2017.

- [26] L. Jia, J. Yin, and X. Ma. Effect of magnetic properties of soft magnetic phase on the energy product of an exchange-spring magnet. *Chinese Physics B*, 23(2):027501, 2014.
- [27] N. M. Saiden, T. Schrefl, H. Davies, and G. Hrkac. Micromagnetic finite element simulation of nanocrystalline  $\alpha$ -Fe/Nd<sub>2</sub>Fe<sub>14</sub>B/Fe<sub>3</sub>B magnets. *Journal of Magnetism and Magnetic Materials*, 365:45–50, 2014.
- [28] X. Fan, S. Guo, K. Chen, R. Chen, D. Lee, and C. You. Tuning Ce distribution for high performed Nd-Ce-Fe-B sintered magnets. *Journal of Magnetism and Magnetic Materials*, 419:394–399, 2016.
- [29] R. Fischer, T. Schrefl, H. Kronmüller, and J. Fidler. Grain-size dependence of remanence and coercive field of isotropic nanocrystalline composite permanent magnets. *Journal of Magnetism and Magnetic Materials*, 153:35–49, 1996.
- [30] T. Schrefl. Remanence and coercivity in isotropic nanocrystalline permanent magnets. *Phys. Rev. B*, 49(9):6100–6110, 1994.
- [31] X. L. Wan, G. P. Zhao, X. F. Zhang, J. Xia, X. C. Zhang, and F. J. Morvan. Hysteresis of misaligned hard-soft grains. *Journal of Magnetism and Magnetic Materials*, 397:181–187, 2016.
- [32] N. Umetsu, A. Sakuma, and Y. Toga. First-principles study of interface magnetic structure in Nd<sub>2</sub>Fe<sub>14</sub>B/Fe,Co exchange spring magnets. *Physical Review B*, 93(1):014408, 2016.
- [33] Daisuke Ogawa, Kunihiro Koike, Shigemi Mizukami, Takamichi Miyazaki, Mikihiko Oogane, Yasuo Ando, and Hiroaki Kato. Negative exchange coupling in Nd<sub>2</sub>Fe<sub>14</sub>B(100)/ $\alpha$ -Fe interface. *Applied Physics Letters*, 107(10):102406, 2015.
- [34] Q. Chen, B. M. Ma, B. Lu, M. Q. Huang, and D. E. Laughlin. A study on the exchange coupling of NdFeB-type nanocomposites using Henkel plots. *Journal of Applied Physics*, 85(8):5917–5919, 1999.
- [35] J. Zhang, S. Y. Zhang, H. W. Zhang, and B. G. Shen. Structure, magnetic properties, and coercivity mechanism of nanocomposite SmCo<sub>5</sub>/ $\alpha$ -Fe magnets prepared by mechanical milling. *Journal of Applied Physics*, 89(10):5601–5605, 2001.
- [36] D.W. Hu, M. Yue, J.H. Zuo, R. Pan, D.T. Zhang, W.Q. Liu, J.X. Zhang, Z.H. Guo, and W. Li. Structure and magnetic properties of bulk anisotropic SmCo<sub>5</sub>/ $\alpha$ -Fe nanocomposite permanent magnets prepared via a bottom up approach. *Journal of Alloys and Compounds*, 538:173–176, 2012.
- [37] S. Tao, Z. Ahmad, P. Zhang, M. Yan, and X. Zheng. Nanocomposite Nd-Y-Fe-B-Mo bulk magnets prepared by injection casting technique. *Journal of Magnetism and Magnetic Materials*, 437:62–66, 2017.

- [38] L. Z. Zhao, Q. Zhou, J. S. Zhang, D. L. Jiao, Z. W. Liu, and J. M. Greneche. A nanocomposite structure in directly cast NdFeB based alloy with low Nd content for potential anisotropic permanent magnets. *JMADE*, 117:326–331, 2017.
- [39] A. M. Gabay, G. C. Hadjipanayis, M. Marinescu, and J. F. Liu. Hot-deformed Sm-Co/Co composite magnets fabricated from powder blends. *Journal of Applied Physics*, 107(9):17–20, 2010.
- [40] E. Fullerton, J. S. Jiang, and S. D. Bader. Hard/soft magnetic heterostructures: model exchange-spring magnets. *Journal of Magnetism and Magnetic Materials*, 200(1-3):392–404, 1999.
- [41] J. Jin, Y. Liu, K. Li, Y. Luo, D. Yu, S. Lu, J. Xie, and B. Lv. Study on Magnetic Behavior of  $\text{Nd}_8\text{Fe}_{84}\text{Ti}_2\text{B}_6$  Nanocomposite by FORC Diagram. *Materials Research*, 18:106–109, 2015.
- [42] O. Isnard, D. Givord, E. Dorolti, V. Pop, L. Nistor, A. Tunyagi, and I. Chicinas. Magnetic and structural behaviour of  $(\text{Nd,Dy})_2\text{Fe}_{14}\text{B}/\alpha\text{-Fe}$  nanocomposites obtained by mechanical milling and annealing. *Journal of Optoelectronics and Advanced Materials*, 10(7):1819–1822, 2008.
- [43] Z. Shiyan, X. Hui, N. Jiansen, W. Hailong, B. Qin, and D. Yuanda. Effect of Gallium Addition on Magnetic Properties of  $\text{Nd}_2\text{Fe}_{14}\text{B}$ -Based/ $\alpha\text{-Fe}$  Nanocomposite Magnets. *Journal of Rare Earths*, 25(1):74–78, 2007.
- [44] S. Zhang, H. Xu, X. Tan, J. Ni, X. Hou, and Y. Dong. Effect of pulsed magnetic field treatment on the magnetic properties for nanocomposite  $\text{Nd}_2\text{Fe}_{14}\text{B}/\alpha\text{-Fe}$  alloys. *Journal of Alloys and Compounds*, 459(1-2):41–44, 2008.
- [45] W. Zhang, B. Shen, Z. Cheng, L. Li, Y. Zhou, and J. Li. Beneficial effect of Gd substitution on magnetic properties of magnetically anisotropic  $\text{SmCo}_5$  ribbons. *Applied Physics Letters*, 79(12):1843, 2001.
- [46] S. Hirose. Elements Strategy toward High-Performance Permanent Magnets free from Critical Elements. *REPM2014*, pages 0–10, 2012.
- [47] H. Fukunaga, R. Horikawa, M. Nakano, T. Yanai, T. Fukuzaki, and K. Abe. Computer Simulations of the Magnetic Properties of Sm-Co / $\alpha\text{-Fe}$  Nanocomposite Magnets With a Core-Shell Structure. *Magnetics, IEEE Transactions on*, 49(7):3240–3243, 2013.
- [48] L.H. Lewis, D.O. Welch, and V. Panchanathan. Curie temperature enhancement of  $\text{Nd}_2\text{Fe}_{14}\text{B}$  in nanocomposite exchange-spring alloys. *Journal of Magnetism and Magnetic Materials*, 175:275–278, 1997.
- [49] M. Rada, J. Lyubina, A. Gebert, O. Gutfleisch, and L. Schultz. Corrosion behavior of Nd-Fe-B/ $\alpha\text{-Fe}$  nanocomposite magnets. *Journal of Magnetism and Magnetic Materials*, 290-291 PA:1251–1254, 2005.

- [50] V. Neu, S. Sawatzki, M. Kopte, Ch Mickel, and L. Schultz. Fully Epitaxial, Exchange Coupled SmCo<sub>5</sub>/Fe Multilayers With Energy Densities above 400 kJ/m<sup>3</sup>. *IEEE TRANSACTIONS ON MAGNETICS*, 48(11):3599–3602, NOV 2012. International Magnetics Conference (INTERMAG), Vancouver, CANADA, MAY 07-11, 2012.
- [51] C. B. Rong, Y. Zhang, M. J. Kramer, and J. P. Liu. Correlation between microstructure and first-order magnetization reversal in the SmCo<sub>5</sub>/α-Fe nanocomposite magnets. *Physics Letters, Section A: General, Atomic and Solid State Physics*, 375(10):1329–1332, 2011.
- [52] J. A. Diego, M. T. Clavaguera-Mora, and N. Clavaguera. Thermodynamic, kinetic and structural mechanisms controlling the formation of nanocrystalline Nd-Fe-B materials. *Materials Science and Engineering A*, 179-80(pt 1):526–530, 1994.
- [53] J. M. Le Breton, R. Lardé, H. Chiron, V. Pop, D. Givord, O. Isnard, and I. Chicinas. A structural investigation of SmCo<sub>5</sub>/Fe nanostructured alloys obtained by high-energy ball milling and subsequent annealing. *Journal of Physics D: Applied Physics*, 43:085001, 2010.
- [54] Z Li, T. Zhang, B. Shen, M. Zhang, F. Hu, and J. Sun. Overcoming of energy barrier for irreversible magnetization in nanocomposite magnets. *Journal of Magnetism and Magnetic Materials*, 422:249–254, 2017.
- [55] E. Dorolti, A. V. Trifu, O. Isnard, I. Chicinas, F. Tolea, M. Valeanu, and V. Pop. Influence of mechanical milling on the physical properties of SmCo<sub>5</sub> / Fe<sub>65</sub>Co<sub>35</sub> type hard / soft magnetic nanocomposite. *Journal of Alloys and Compounds*, 560:189–194, 2013.
- [56] A. Hosokawa, K. Takagi, and T. Kuriiwa. Nanocomposite Nd-Fe-Ti-B magnets produced by melt spinning and flash annealing. *Journal of Magnetism and Magnetic Materials*, 439:220–227, 2017.
- [57] X. Tang, X. Chen, R. Chen, and A. Yan. Polycrystalline Nd<sub>2</sub>Fe<sub>14</sub>B/α-Fe nanocomposite flakes with a sub-micro/nanometre thickness prepared by surfactant-assisted high-energy ball milling. *Journal of Alloys and Compounds*, 644:562–569, 2015.
- [58] P. Saravanan, R. Gopalan, D. Sivaprahasam, and V. Chandrasekaran. Effect of sintering temperature on the structure and magnetic properties of SmCo<sub>5</sub>/Fe nanocomposite magnets prepared by spark plasma sintering. *Intermetallics*, 42:199–204, 2013.
- [59] V. Pop, E. Dorolti, C. Vaju, E. Gautron, O. Isnard, J. M. Le Breton, and I. Chicinas. Structural and Magnetic Behaviour of SmCo<sub>5</sub>/α-Fe Nanocomposites Obtained By Mechanical Milling. *Romanian Journal of Physics*, 55:127–136, 2010.
- [60] V. Pop, I. Chicinas, and N. Jumate. *Fizica Materialelor - Metode Experimentale*. Presa Universitara Clujeana, Cluj-Napoca, 2001.

- [61] H. Mayot. *Contribution à l'étude cristallographique et magnétique de composés intermétalliques RCoB et RFeB (R=élément de terres rares)*. PhD thesis, INSTITUT NEEL, CNRS UJF, 2008.
- [62] E Gaffet and G Le Caër. *Mechanical processing for nanomaterials*, volume X. 2004.
- [63] C. Suryanarayana. Mechanical alloying and milling. *Progress in Materials Science*, 46:1–184, 2001.
- [64] N. Burgio, A. Iasonna, M. Magini, S. Martelli, and F. Padella. Mechanical Alloying of the Fe-Zr System. Correlation between Input Energy and End Products. *Il Nuovo Cimento*, 13 D(4):459–476, 1991.
- [65] M. Abdellaoui and E. Gaffet. The physics of mechanical alloying in a planetary ball mill: Mathematical treatment. *Acta Metallurgica Et Materialia*, 43(3):1087–1098, 1995.
- [66] H. Ghayour, M. Abdellahi, and M. Bahmanpour. Optimization of the high energy ball-milling: Modeling and parametric study. *Powder Technology*, 291:7–13, 2016.
- [67] Yan Chen and Yan Chen. *Design of Structural Mechanisms*. PhD thesis, University of Oxford - St Hughs College, 2003.
- [68] P. Scherrer. Bestimmung der Grösse und der Inneren Struktur von Kolloidteilchen Mittels Röntgenstrahlen, *Nachrichten von der Gesellschaft der Wissenschaften, Göttingen. Mathematisch-Physikalische Klasse*, 2:98 – 100, 1918.
- [69] I.D. Mayergoyz. *Mathematical Models of Hysteresis*. Springer, 1991.
- [70] G. Bertotti. *Hysteresis in Magnetism: For Physicists, Materials Scientists, and Engineers*, 1998.
- [71] D. Maurice and T. H. Courtney. Modeling of mechanical alloying: Part II. Development of computational modeling programs. *Metallurgical and Materials Transactions A*, 26(9):2431–2435, 1995.
- [72] W. Pompe, H. J. Herrmann, and S. Roux. Statistical models for the fracture of disordered media. *Crystal Research and Technology*, 26(8), jan 1991.